iScience

CellPress
OPEN ACCESS

Article

Combined epigenetic and metabolic treatments overcome differentiation blockade in acute myeloid leukemia

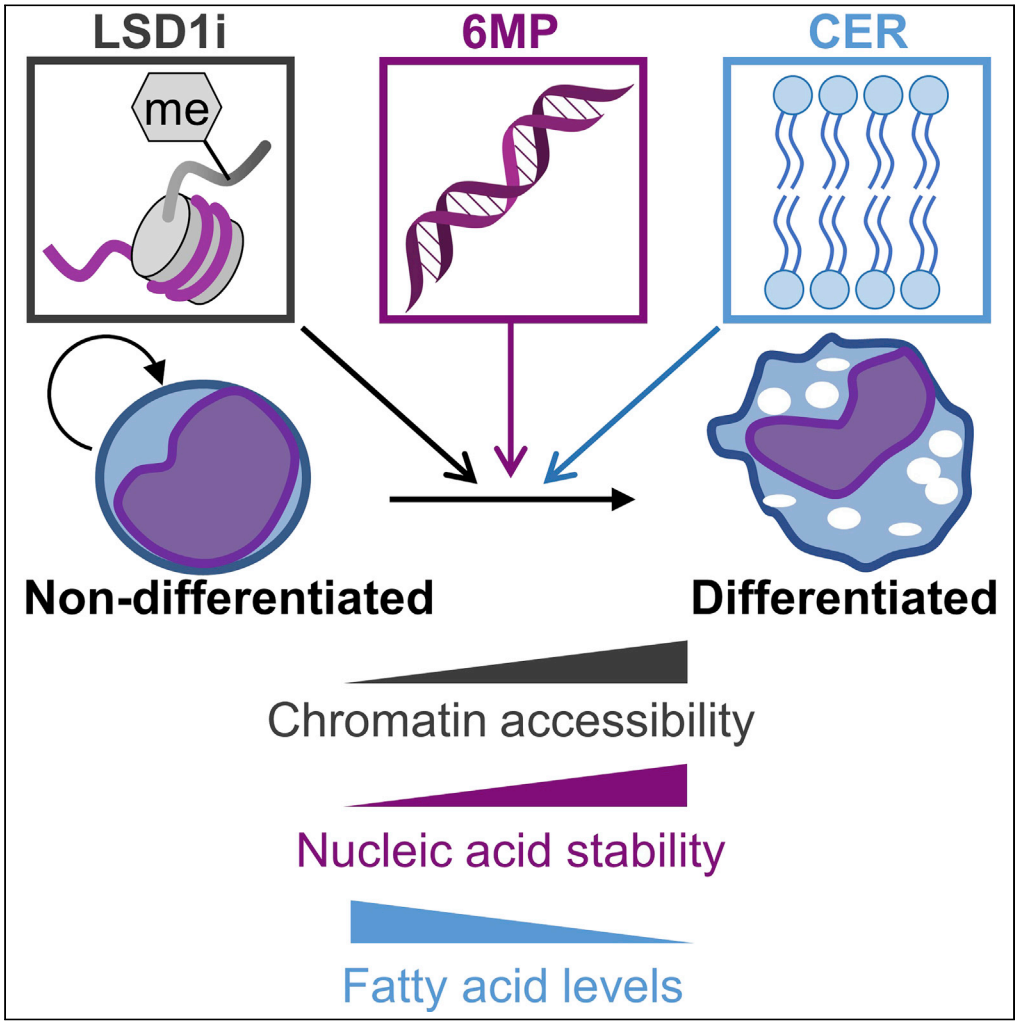

Barry M. Zee, Kamrine E. Poels, Cong-Hui Yao, ..., Marcia C. Haigis, Franziska Michor, Yang Shi

yang.shi@ludwig.ox.ac.uk

Highlights

Combined epigenetic and metabolic perturbations induce myeloid differentiation

Combination treatment alters nucleotide, lipid, and gene expression profiles

Combination treatment induces differentiation of human acute myeloid leukemia cells

Zee et al., iScience *24*, 102651
June 25, 2021
https://doi.org/10.1016/j.isci.2021.102651

iScience

CellPress
OPEN ACCESS

Article

Combined epigenetic and metabolic treatments overcome differentiation blockade in acute myeloid leukemia

Barry M. Zee,[1,2] Kamrine E. Poels,[3,4] Cong-Hui Yao,[5] Kimihito C. Kawabata,[6] Gongwei Wu,[7] Cihangir Duy,[8,9] William D. Jacobus,[1] Elizabeth Senior,[1] Jennifer E. Endress,[5] Ashwini Jambhekar,[1,10,11] Scott B. Lovitch,[12] Jiexian Ma,[1] Abhinav Dhall,[1,2] Isaac S. Harris,[5] M. Andres Blanco,[1] David B. Sykes,[13] Jonathan D. Licht,[14] David M. Weinstock,[7,15] Ari Melnick,[6] Marcia C. Haigis,[5] Franziska Michor,[3,4,11,16,17,18] and Yang Shi[1,2,19,*]

SUMMARY

A hallmark of acute myeloid leukemia (AML) is the inability of self-renewing malignant cells to mature into a non-dividing terminally differentiated state. This differentiation block has been linked to dysregulation of multiple cellular processes, including transcriptional, chromatin, and metabolic regulation. The transcription factor HOXA9 and the histone demethylase LSD1 are examples of such regulators that promote differentiation blockade in AML. To identify metabolic targets that interact with LSD1 inhibition to promote myeloid maturation, we screened a small molecule library to identify druggable substrates. We found that differentiation caused by LSD1 inhibition is enhanced by combined perturbation of purine nucleotide salvage and *de novo* lipogenesis pathways, and identified multiple lines of evidence to support the specificity of these pathways and suggest a potential basis of how perturbation of these pathways may interact synergistically to promote myeloid differentiation. In sum, these findings suggest potential drug combination strategies in the treatment of AML.

INTRODUCTION

Differentiation arrest is a clinically relevant hallmark of acute myeloid leukemia (AML), resulting in accumulation of undifferentiated myeloid precursors (blasts) that overtake the bone marrow, and in morbidity and mortality due to insufficient numbers of mature myeloid cells (de Thé, 2018). Accordingly, a longstanding concept in the treatment of AML is to induce committed maturation of these cancerous cells, promoting clearance of the malignant clones and allowing normal progenitors to repopulate the marrow. Such an approach could yield therapies that are less toxic than the current standard of care of chemotherapy and hematopoietic stem cell transplantation, which is often unsuitable for elderly patients and those with significant comorbidities (Döhner et al., 2010; Juliusson 2011; Thomas and le Jeune, 2017). However, while this strategy has proven effective in AML subtypes with specific driver mutations, most notably acute promyelocytic leukemia with PML-RARA fusion and AML with IDH1/IDH2 mutation, attempts to extend this approach to treatment of AML more generally have proven unsuccessful to date.

AML differentiation arrest involves regulation across multiple pathways. A common feature of AML transcriptional profiles is constitutive activation of *HOXA9*, which encodes for a transcription factor that positively and negatively regulates proliferation- and differentiation-associated genes, respectively (Collins et al., 2014). Typically, *HOXA9* expression decreases as progenitor cells mature. Yet in nearly half of patients with AML *HOXA9* remains highly expressed and is a predictor for poor prognosis (Gao et al., 2016). Interestingly, *HOXA9* is required for oncogenesis in AML subtypes characterized by *MLL* (*KMT2A*) fusion oncogenes (Faber et al., 2009). In addition, altered epigenetic patterns influence the AML differentiation blockade. Consistent with published findings (Schenk et al., 2012) (McGrath et al., 2016) (Cusan et al., 2018), we also identified a role for the histone demethylase LSD1 (KDM1A) in maintaining the myeloid differentiation blockade. LSD1 promotes a repressed chromatin state. Upon LSD1 inhibition, chromatin proteins with specialized domains recognize regions previously repressed by LSD1 and promote a more accessible, non-repressed state. Together with the pioneer transcription factors C/EBPα and PU.1, LSD1

[1]Division of Newborn Medicine, Boston Children's Hospital, Boston, MA 02115, USA

[2]Ludwig Institute for Cancer Research, Oxford University, OX3 7DQ, UK

[3]Department of Data Science, Dana Farber Cancer Institute, Boston, MA 02215, USA

[4]Department of Biostatistics, Harvard T.H. Chan School of Public Health, Boston, MA 02115, USA

[5]Department of Cell Biology, Harvard Medical School, Boston, MA 02115, USA

[6]Division of Hematology-Medical Oncology, Weill Cornell Medicine, New York, NY 10065, USA

[7]Department of Medical Oncology, Dana-Farber Cancer Institute, Boston, MA 02215, USA

[8]Cancer Signaling and Epigenetics Program, Institute for Cancer Research, Fox Chase Cancer Center, Philadelphia, PA 19111, USA

[9]Cancer Epigenetics Institute, Fox Chase Cancer Center, Philadelphia, PA 19111, USA

[10]Department of Systems Biology, Harvard Medical School, Boston, MA 02115, USA

[11]The Ludwig Center at Harvard, Boston, MA 02115, USA

[12]Department of Pathology, Brigham and Women's Hospital, Boston, MA 02115, USA

[13]Center for Regenerative Medicine, Massachusetts General Hospital, Boston, MA 02114, USA

Continued

inhibition induces a pro-differentiation program. Thus, altered epigenetic regulation promotes leukemia in part through dysregulation of transcriptional pathways that induce myeloid differentiation.

Inhibitors against numerous chromatin factors are available, making them therapeutically attractive targets. However, developing therapies targeting these pathways has been challenging due to the essential role of chromatin factors such as LSD1 in the normal myeloid differentiation program (Kerenyi et al., 2013). A recent AML phase 1 clinical trial (NCT02177812) using an LSD1 inhibitor was terminated in part due to toxicity. One strategy to improve drug tolerability is to use lower doses in combination with other compounds for an enhanced phenotype, in this context, enhanced differentiation. Generally, combination therapies target distinct substrates to minimize selection of resistant clones. It is sensible, then, to combine epigenetic inhibitors with non-epigenetic inhibitors that target AML-relevant pathways. While specific epigenetic components such as LSD1 regulate transcriptional networks that block maturation, specific metabolic fluxes also support the state of self-renewal (Kreitz et al., 2019). For instance, leukemic cells induced to differentiate downregulate *de novo* synthesis of fatty acids and proteins, suggesting a correlation between differentiation status and metabolic flux (Vlodavsky et al., 1975) (Burns, 1975). These examples raise the broader question of how, if at all, specific metabolic pathways interact with chromatin regulation in the context of the AML differentiation blockade. Here, we report that targeting the purine and fatty acid metabolic pathways in combination with LSD1 inhibition bypasses the differentiation arrest program and induces maturation. This work lays the groundwork for potential clinical testing of LSD1i-based combination treatment for AML.

RESULTS

LSD1 inhibition induces limited differentiation in granulocyte-monocyte progenitors

To study the differentiation block in AMLs, we used a genetically defined driver of leukemia whose expression can be controlled to manipulate the cellular differentiation status. We used a recently reported mouse granulocyte-monocyte progenitor (GMP) line that expresses an ER-HOXA9 transgene, with the estrogen receptor (ER) hormone-binding domain providing estradiol (E2)-dependent posttranslational control of HOXA9. This genetically defined line is referred to herein as ER-HOXA9 cells (Sykes et al., 2016). While these cells are not functionally leukemic, when cultured with E2 and stem cell factor (SCF) to maintain proliferative and progenitor potential, respectively, these cells model an AML-like differentiation blockade at the early GMP stage. The endogenous lysozyme (*Lyz2*) promoter in these cells drives expression of a GFP reporter during myeloid differentiation and serves as a differentiation reporter (Faust et al., 2000) (Figure 1A).

We first tested whether LSD1 inhibition induced differentiation in ER-HOXA9 cells, as reported for other AML models (Harris et al., 2012) (Schenk et al., 2012) (McGrath et al., 2016) (Cusan et al., 2018). Treatment of ER-HOXA9 cells with 10nM GSK-LSD1, an irreversible and specific LSD1 inhibitor (LSD1i), significantly induced differentiation relative to vehicle treatment ($p_{adj} = 3 \times 10^{-3}$) (Figure S1) (Mohammad et al., 2015). The percentage of differentiated cells (approximately 6–9%) remained largely unchanged at higher drug concentrations from 100nM to 10μM LSD1i. Treating cells with another LSD1 inhibitor, tranylcypromine (TCP), increased the fraction of differentiated cells at 10 μM ($p_{adj} = 1 \times 10^{-2}$) (Schmidt and McCafferty, 2007) (Figure S1). Thus, our data support published findings that chemical inhibition of LSD1 promotes myeloid differentiation (Harris et al., 2012) (Schenk et al., 2012) (McGrath et al., 2016) (Cusan et al., 2018).

A chemical screen identifies metabolic drugs that enhance LSD1i induction of differentiation

Because ER-HOXA9 differentiation induced by LSD1 inhibition is less potent than that induced by HOXA9 inactivation (6–9% compared to >90%, respectively) (Sykes et al., 2016), we screened a library of small molecules targeting metabolic pathways for enhancement of LSD1i-induced differentiation (Figure 1A) (Harris et al., 2019). We identified 6-mercaptopurine (6MP) and cerulenin (CER) as two candidates that, when combined with LSD1i, promoted ER-HOXA9 differentiation to a greater extent than LSD1i alone and to a similar extent as cytarabine did, a known lysozyme inducer (Krystosek and Sachs, 1976) (Figure 1B). 6MP (Figure 1C) is a synthetic purine that is metabolized by the purine salvage pathway to yield nucleotides that can incorporate into RNA or DNA (Figure S2) (Elion et al., 1953). Unmodified 6MP-derived nucleotides pair with cytosine (Bohon and de los Santos, 2005), but upon methylation or oxidation of the sulfur atom, they pair with uracil or thymine (Yuan and Wang, 2008). The natural product CER (Figure 1C) targets fatty acid synthase and reduces incorporation of acetate into lipids (Nomura et al., 1972) (Goldberg et al., 1973). LSD1i combinations with these drugs also promoted differentiation in the ER-HOXA9-related mouse cell line

[14]Division of Hematology and Oncology, University of Florida Health Care Center, Gainesville, FL 32610, USA

[15]Cancer Biology Program, Broad Institute of MIT and Harvard University, Cambridge, MA 02142, USA

[16]Department of Stem Cell and Regenerative Biology, Harvard University, Cambridge, MA 02138, USA

[17]The Broad Institute of MIT and Harvard, Cambridge, MA 02139, USA

[18]The Center for Cancer Evolution, Dana-Farber Cancer Institute, Boston, MA 02215, USA

[19]Lead contact

*Correspondence: yang.shi@ludwig.ox.ac.uk

https://doi.org/10.1016/j.isci.2021.102651

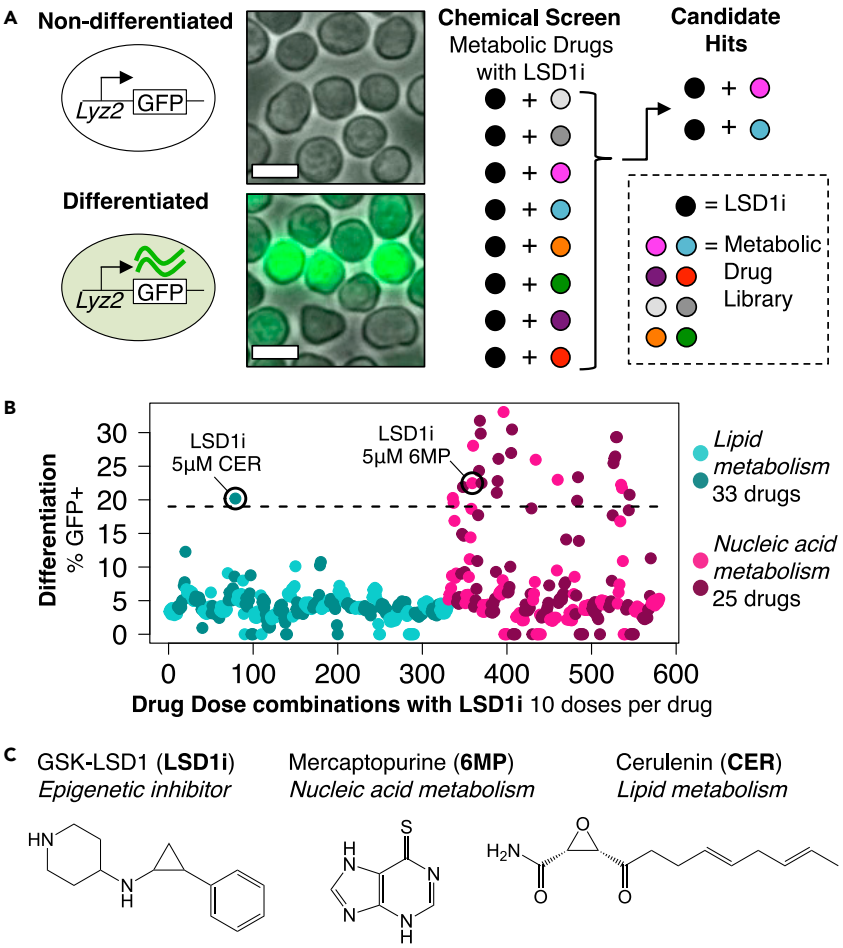

Figure 1. Small molecule screen identifies two compounds that enhance LSD1i-mediated differentiation of ER-HOXA9 cells

(A) ER-HOXA9 cells were treated with GSK-LSD1 (LSD1i) combined with individual drugs from a compound library to determine which combinations induced differentiation to greater level than LSD1i treatment alone. Insert shows merged fluorescent images of ER-HOXA9 cells in non-differentiated and differentiated states following 50nM LSD1i treatment (White bar = 10 microns). Differentiated cells activate the *Lyz2-GFP* reporter, which provides a readout for differentiation.
(B) Compound screen measuring differentiation of ER-HOXA9 cells treated with combinations of LSD1i with lipid (left) and nucleic acid (right) metabolism drugs for five days. Alternating bands of color represent a different drug, where individual dots (average of two replicates) represent a specific dose of that drug. Drug doses that significantly reduced viability (i.e. $\leq$ 10% of total cells were live) were assigned 0% differentiation. Horizontal line at 19% differentiation, which is the average efficiency observed with the cytarabine positive control, designated the significance threshold. Two candidates, mercaptopurine (6MP) and cerulenin (CER) are highlighted. See Table S2 for full compound screen information.
(C) Chemical structures of LSD1i, 6MP, and CER.
See also Figures S1 and S2 and Table S1.

ER-HOXB8 (Wang et al., 2006) (Figure S3) and in the human cell line U937 (Figure S4), and the drug combinations reduced proliferation in a panel of myeloid and lymphoid cell lines (Figure S5). Thus, our screen suggests two compounds, when combined with LSD1i, increase the fraction of differentiated cells.

Time and dose dependence of differentiation response to epigenetic and metabolic perturbations

To assess the timing and extent of differentiation induced by these drug combinations, we treated ER-HOXA9 cells with different doses and combinations of LSD1i, 6MP, and CER for one to five days and assayed proliferation and differentiation at each day (Figure 2A) (Figure S6). Cells in the vehicle-only group increased in numbers by approximately 150 times the initial density after five days (consistent with a

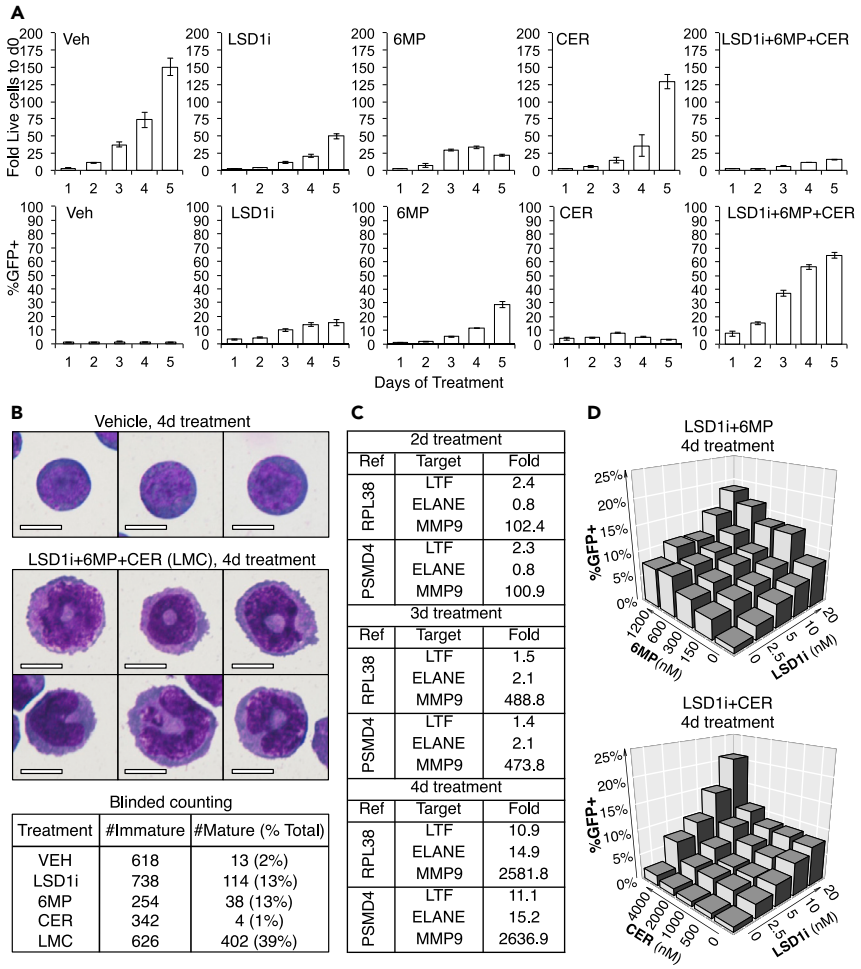

Figure 2. 6MP and CER suppress proliferation and enhance differentiation in combination with LSD1i

(A) Time course measurement of proliferation (top) and differentiation (bottom) status of ER-HOXA9 cells treated with 200nM LSD1i, 5μM 6MP, and 5μM CER for one to five days as single or triple combinations. Proliferation was measured as live cell numbers relative to initial cell numbers at day 0 (approximately 2500 live cells), where for example a value of 25 indicates 25 × 2500 = 62,500 live cells. Differentiation was measured as percentage of cells positive for Lyz2-GFP. Bars represent average of three to four technical replicates, and error bars represent standard deviation. See Table S6 for data.

(B) ER-HOXA9 cells treated with LMC combination (200nM LSD1i, 5μM 6MP, and 5μM CER) display morphologies consistent with mature murine leukocytes. Images were acquired at 120× magnification (White bar = 10 microns). Cells treated with vehicle or drugs were classified as immature or mature cells in blinded manner.

(C) Genes related to neutrophil granule formation (Target) were quantified for expression changes in ER-HOXA9 cells treated with vehicle or LMC combination (200nM LSD1i, 5μM 6MP, and 5μM CER) for two to four days. Values represent average of two replicates and normalized to the specified housekeeping reference genes (Ref).

(D) Differentiation status of ER-HOXA9 cells after treatment with multiple doses of LSD1i and 6MP (top) or with LSD1i and CER (bottom) as double drug combinations for four days. Bars represent average of five to six technical replicates.

See also Figures S3–S8 and Tables S3–S7 and S18.

doubling time of approximately 16 hr), and displayed a spontaneous differentiation rate of approximately 1%. In comparison, cells treated with LSD1i or 6MP increased in numbers by 50 or 22 times the initial density, respectively, while cells treated with CER increased in numbers at similar rate as controls. The triple combination suppressed proliferation more than any individual drug, with cells increasing by approximately 15 times the initial density, without causing extensive cell death. Because reduced proliferation itself does not activate the mouse lysozyme promoter (Krystosek and Sachs, 1976), we used LYZ-GFP expression to assess differentiation status. After one day of treatment, there was no significant induction of differentiation (Figure S6C). After two days of treatment, we observed a significant differentiation response with LSD1i and CER double combinations, while LSD1i and 6MP double combinations did not

induce a significantly greater response from vehicle until day 3 of treatment. The triple drug combination induced a significantly greater response over the double drug combinations after four days of treatment. We observed this pattern of the double and triple combinations increasing differentiation relative to vehicle or single drug treatment across multiple ER-HOXA9 clones (Figure S7). To complement the GFP-reporter data, we assayed differentiation status of ER-HOXA9 cells by morphological features (Figure 2B) and expression of genes coding for neutrophil granule components (Figure 2C) (Abdel-Aziz and Minucci, 2019). Both assays suggested that the drug combinations induced myeloid maturation, with similar results in ER-HOXB8 and U937 lines (Figures S3B, S3C, S4B, and S4C). As overall levels of cell death in drug-treated cells were low (Figure 2A) and the absolute numbers of differentiated cells increased following treatment (Table S6), it is unlikely that the increase in the proportion of differentiated cells results from selective toxicity of the drugs to undifferentiated cells. Rather, it is likely that the drugs promote differentiation through more direct mechanisms.

Finally, we identified the lowest doses of each drug sufficient to significantly increase differentiation (Figure 2D). Treatment with 5nM LSD1i and 0.3μM 6MP or with 2.5nM LSD1i and 4μM CER as double combinations induced a significantly greater fraction of differentiated ER-HOXA9 cells than did treatment with the same drug doses individually. Modeling the drug response based on Bliss interactions suggests the drugs synergistically reduced the proportion of live, non-differentiated cells (Figure S8). In summary, our results support the notion that epigenetic, nucleic acid, and lipid regulation can be inhibited in a combinatorial manner to reproducibly bypass the differentiation blockade.

Stability of drugs in various media does not correlate with maintenance of differentiation response

Our data suggest that differentiation occurs soon after CER treatment and more gradually after 6MP treatment (Figure S6C). To investigate whether the different timescales might be due to different rates of drug metabolism, we quantified drug concentrations over time. We measured CER to have a half-life of approximately 2 days in media and 1 hr in plasma, while LSD1i and 6MP both have a half-life of approximately 3–4 days in media and over 3 hr in plasma (Figure S9). Our results suggest that cells experience different molar ratios of the drugs across the time span of an experiment, which may affect the timing of differentiation.

We next tested whether the drugs were required for maintaining the differentiation program once it was initiated. Since CER was the least stable, we predicted that CER would exert its effects early in the process and be dispensable later. To test this hypothesis, we primed ER-HOXA9 cells with a single drug for two days, washed drug away, and subsequently treated cells with the other drugs for another two days (Figure S10A). Contrary to our expectation, initial CER treatment followed by LSD1i and 6MP induced less differentiation than continuous triple drug combination. In contrast, initial 6MP treatment followed by LSD1i and CER induced similar differentiation as continuous triple drug combination. To further characterize this response, we treated cells with various combinations of drugs for two days, replaced with drug-free media, and measured the fraction of differentiated cells at the time of washout and again two or four days later (days 0, 2, and 4 of the experiment, respectively) (Figure S10B). CER induced a transient response at two days, which returned to control levels after washout. The differentiation response was enhanced at the time of washout but not maintained subsequently when CER was combined with LSD1i. By contrast, the differentiation responses induced by LSD1i and 6MP did not decrease following washout. These experiments suggest that, despite the short half-life of CER, it continues to promote differentiation late into the process. 6MP is mainly required during the early stages of differentiation despite its longer half-life, and only LSD1i and CER are required beyond the second day to promote differentiation.

Drugs that target pathways similar to LSD1i, 6MP, and CER can also modulate differentiation

To investigate whether the differentiation observed above resulted from any off-target drug effects, we repeated the studies using other drugs with similar mechanisms of action. Substituting TCP for GSK-LSD1 in the triple combination induced significantly greater differentiation than any single treatment (Figure S11). Three different analogs—6-thioguanine, thioguanosine (TG), and deoxythioguanosine (dTG)—each enhanced differentiation when combined with LSD1i (Figure S12). Notably, 6-thioguanine scored as a hit in our original screen (Table S2). Finally, inhibiting acetyl-CoA synthase (ACC), an enzyme that acts upstream of the CER target fatty acid synthase, with 2 different drugs (TOFA or ND630) (McCune and Harris, 1979) (Harriman et al., 2016) each in combination with LSD1i induced differentiation (TOFA) (Figures S13A and S13 B) and suppressed proliferation (ND630) (Figure S13C). Collectively, these results support the hypothesis that the use of multiple

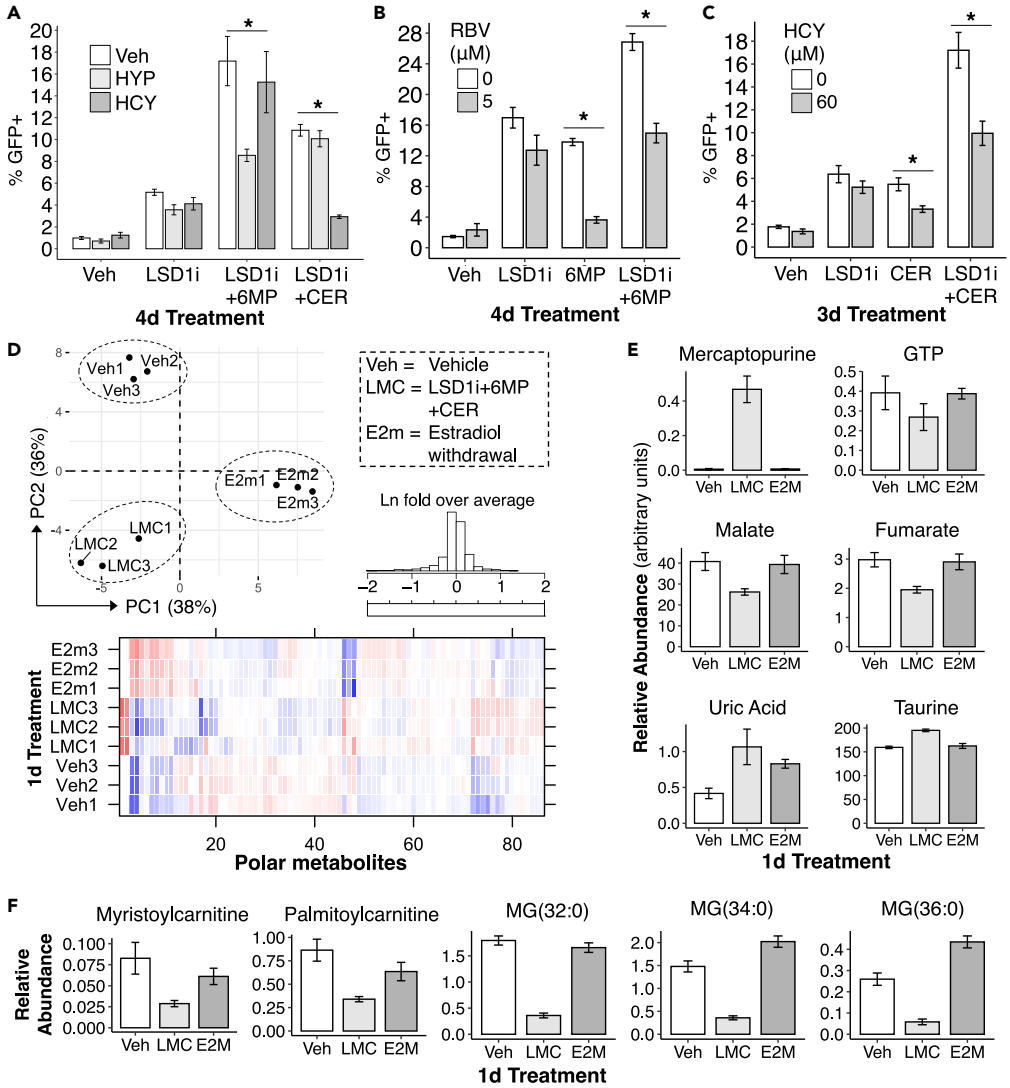

Figure 3. Metabolic profiling and suppression of the differentiation response to drugs

(A) ER-HOXA9 cells were treated with combinations of 200nM LSD1i, 5μM 6MP, and 5μM CER and suppressed with vehicle (white), 10μM HYP (light gray) or 1mM HCY (dark gray) for four days. Differentiation for Panels A-C was assessed by Lyz2-GFP expression. Bars and vertical lines represent average and standard deviation, respectively, of eight technical replicates. Asterisks in Panels A-C represent significant differences (*$p_{adj} < 0.01$) as determined by Games-Howell test. See Table S12 for data for Panels A-C.

(B) ER-HOXA9 cells treated with vehicle, 200nM LSD1i, 2.5 μM 6MP, and double combination of both drugs were co-incubated with vehicle or 5μM ribavirin (RBV) for four days. Bar and vertical lines represent average and standard deviation of six technical replicates.

(C) ER-HOXA9 cells treated with vehicle, 200nM LSD1i, 5μM CER, or double combination of both drugs were co-incubated with or without 60μM (HCY) for three days. Bar and vertical lines represent average and standard deviation of eight technical replicates.

(D) Principal component analysis of the relative abundances of polar metabolites extracted from ER-HOXA9 cells treated with vehicle (VEH), triple drug combination (LMC, at 200nM LSD1i, 5μM 6MP, and 5μM CER), or estradiol withdrawal (E2M). The heatmap depicts the natural log fold change of the abundance of a given metabolite over the average abundance of that metabolite across all samples (red and blue represent enriched or depleted over average). Histogram represents distribution of fold changes across all metabolites and treatments. See Table S13 for data.

(E) Relative abundances of select polar metabolites extracted from ER-HOXA9 cells treated with vehicle (white), drugs (light gray), or estradiol withdrawal (dark gray). Bars and vertical lines represent mean and standard deviation of three replicates.

Figure 3. *Continued*
(F) Relative abundances of select acylcarnitine and monoglyceride species from ER-HOXA9 cells treated with vehicle (white), drugs (light gray), or estradiol withdrawal (dark gray). Bars and vertical lines represent mean and standard deviation of three replicates.
See also Figures S9–S16 and Tables S8–S14.

inhibitors, which target epigenetic, nucleic acid, and fatty acid pathways, enhances the differentiation and proliferation response.

To further confirm the specificity and mechanisms of actions of the drugs in promoting differentiation, we investigated whether we could suppress differentiation in a mechanistically rational manner. We first tested various aspects of 6MP metabolism for their effects on differentiation. Blocking 6MP excretion with allopurinol, which inhibits xanthine oxidase (Figure S2) (Lennard, 1992), had no effects on differentiation induced by 6MP (Table S12). By contrast, blocking 6MP uptake with the competitive inhibitor hypoxanthine (HYP) (Figure 3A) (Ward et al., 2000) or blocking 6MP activation with the inosine monophosphate dehydrogenase inhibitor ribavirin (RBV) (Figure 3B) (Leyssen et al., 2005) reduced differentiation caused by 6MP or LSD1i+6MP double combination. HYP itself did not induce differentiation (Figure S14) or inhibit differentiation induced by LSD1i + CER double combination, suggesting specificity of the HYP treatment (Figure 3A). The effects on differentiation by CER, which suppresses fatty acid synthesis, were suppressed by homocysteine (HCY) (Figure S2), which activates fatty acid synthesis genes (Lee et al., 2012) (Visram et al., 2018) (Werstuck et al., 2001). The effects of HCY on CER-induced differentiation were seen both in the presence and absence of LSD1i (Figure 3C). In summary, we found that blocking the metabolism of 6MP and CER suppresses the corresponding differentiation responses. These results suggest that the observed differentiation phenotypes arise from the expected on-target effects.

Metabolic profiling reveals drug-specific patterns during differentiation

While we found that metabolic perturbations overcome the differentiation block induced by HOXA9 expression, it remained unclear which specific metabolic changes accompany cell maturation. To address this question and distinguish changes induced by the triple drug combination from those occurring generally in response to differentiation, we treated cells with vehicle, triple drug combination (LSD1i, 6MP, and CER), or E2 withdrawal to inactivate the HOXA9 transgene, and performed metabolomic analysis one day after treatment to capture the immediate and potentially direct effects. All three treatments induced discrete metabolomic responses (Figure 3D and Table S13). Several unique metabolic changes in response to the triple drug treatment were observed, including decrease in GTP (Figure 3E); decrease in acylcarnitine species such as myristoylcarnitine (C14:0) and palmitoylcarnitine (C16:0); and decrease in monoglyceride lipid species (Figures 3F and S15). The first change likely reflects interference with guanine processing by 6MP (Scholar et al., 1972), while the latter two likely reflect FASN inhibition by CER (Thupari et al., 2001). These data suggest that differentiation induced by drugs leads to metabolic responses that are distinct from differentiation induced by HOXA9 inactivation, although further characterization is needed to assay the relevance of specific metabolite changes to differentiation.

Genomic analyses reveal differentiation response induced by drug combinations

To complement the studies on the metabolic responses to drug treatment, we next performed ATAC-seq and RNA-seq experiments to characterize the genomic and transcriptomic responses of ER-HOXA9 cells to drug treatment. Changes in chromatin accessibility of promoters and other regulatory regions often precede changes in transcriptional output of the corresponding genes. To capture the most direct effects, we performed ATAC-seq after two days of treatment and RNA-seq after three days of treatment. We found the triple drug combination (LSD1i, 6MP, and CER) induced accessibility of a greater number of promoters than did treatment with any of the drugs used individually (Figure S16A) (Table S14). Treatment with 6MP or CER alone did not increase promoter accessibility. The majority of protein-coding promoters that gained accessibility with LSD1i treatment (70 of 86) also gained accessibility with triple drug treatment (Figure S16B) and displayed, on average, a greater increase in the magnitude of accessibility with triple drug treatment compared to single LSD1i treatment (Figure S16C). The promoters whose activation was enhanced by the triple drug treatment represented diverse pathways including macromolecule metabolism, response to wounding, and signal transduction (Table S14). Genes with increased promoter accessibility were broadly associated with increased transcription, and approximately a fifth of these genes reached biological significance (Figure S16D). The significantly increased genes include matrix metalloproteinases MMP8

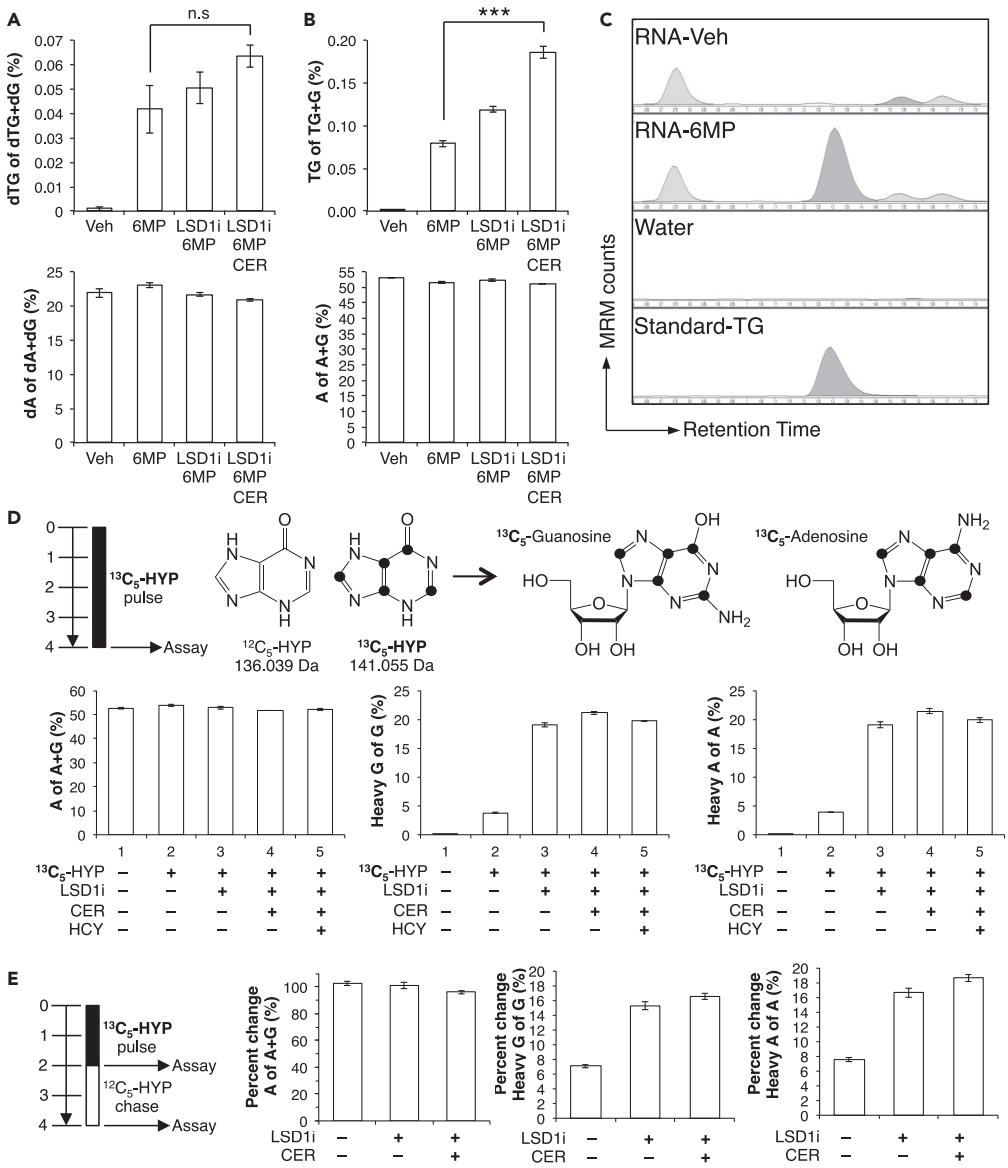

Figure 4. 6MP incorporates into nucleic acids

(A) LC-MS analysis of deoxythioguanosine (dTG) and other deoxynucleotides processed from ER-HOXA9 cells treated with vehicle, single drug (5μM 6MP), double drug combination (200nM LSD1i and 5μM 6MP), and triple drug combination (200nM LSD1i, 5μM 6MP, and 5μM CER) for four days. Levels of dTG were normalized to deoxyguanosine. To access variability across conditions, levels of deoxyadenosine were compared to deoxyguanosine. Bar and vertical lines represent average and standard deviation of three technical replicates. See Table S16 for data.

(B) LC-MS analysis of thioguanosine (TG) and other nucleotides processed from ER-HOXA9 cells treated with vehicle, single drug (5μM 6MP), double drug combination (200nM LSD1i and 5μM 6MP), and triple drug combination (200nM LSD1i, 5μM 6MP, and 5μM CER) for four days. Levels of TG were normalized to guanosine. See Figure S18 for biological replicate. Bar and vertical lines represent average and standard deviation of three technical replicates, and asterisks represent significant differences (***$p_{adj} < 0.0005$) as determined by t test.

(C) HPLC elution profiles of RNA-derived nucleosides from ER-HOXA9 cells treated with vehicle or 5μM 6MP. A water-only sample served as a negative control and thioguanosine standard served as a positive control. Note the similar retention times between the standard and the highlighted peak in the 6MP-treated sample.

(D) Heavy hypoxanthine (HYP) was used as a tracer for purine salvage in total RNA. Black circles represent the ^{13}C carbon isotopes. ER-HOXA9 cells were incubated without heavy HYP as a negative control, or with 5μM heavy HYP combined with various drug combinations for four days. Heavy guanosine and adenosine were normalized to the respective light nucleosides to determine their relative abundance. To assess variability across conditions, levels of total adenosine were

Figure 4. *Continued*
compared to total guanosine (heavy and light). Bar and vertical lines represent average and standard deviation of three replicates.
(E) Pulse-chase experiment of $^{13}C_5$-HYP labeling of guanosine and adenosine in total RNA, where cells were incubated with 5μM $^{13}C_5$-HYP for 2 days, followed by 5μM $^{12}C_5$-HYP for 2 more days. Heavy guanosine and adenosine were normalized to the respective light nucleosides to determine their relative abundance, and the change in abundance before and after chase was determined. Bar and vertical lines represent average and standard deviation of three replicates.
See also Figures S17 and S18 and Tables 15 and S16.

and MMP12, and microsomal glutathione transferase MGST1, which perform important functions for mature myeloid cells (Chou et al., 2016) (Bräutigam et al., 2018). These results suggest potential concordance between chromatin accessibility and gene transcriptional responses with drug treatment.

Incorporation of mercaptopurine into nucleic acids is enhanced with combined epigenetic perturbation

To investigate how triple drug treatment might contribute to the genomic and transcriptional changes described above, we assessed incorporation of the 6MP-derived nucleotides dTG and TG into genomic DNA (gDNA) and total RNA, respectively (Figure S17). We found that 6MP-derived nucleotides readily incorporated into DNA (Figure 4A) and RNA (Figures 4B, 4C, and S18) despite an overall reduction in proliferation, which generally suppresses nucleotide incorporation (Weber and Rublin, 1971) (Neese et al., 2002). Incorporation into RNA was enhanced by co-treatment with LSD1i and CER (Figure 4B). Similar results were obtained in U937 cells (Figure S18B). These results suggested that purine salvage was increased by LSD1i + CER treatment, which we observed directly by incubating cells with labeled hypoxanthine ($^{13}C_5$-HYP), a molecule that does not affect differentiation on its own (Figure 3A). Incorporation of $^{13}C_5$-HYP as $^{13}C_5$-guanosine and $^{13}C_5$-adenosine increased in cells co-treated with LSD1i + CER (Figure 4D), suggesting that perturbing epigenetic and lipogenic pathways favors incorporation of exogenous nucleotides even under conditions that normally suppress it. Some of the TG incorporation in RNA could be attributed to decreased RNA turnover: a pulse-chase experiment using $^{13}C_5$-HYP revealed that 6–8% of the initial levels of isotope remained in RNA after a 2-day chase of control cells, whereas 16–18% remained in drug-treated cells (Figure 4E). The increased levels of remaining heavy isotope support the hypothesis that drug treatment increased total RNA stability, potentially because of the reduction in proliferation as cells differentiate. Whether increased stability is sufficient to fully account for the increased level of TG and dTG incorporation will need to be characterized in future experiments.

Mathematical modeling of treatment response of leukemia *in vivo*

Using data collected from the *in vitro* experiments with ER-HOXA9 cells, we next modeled the pharmacodynamic induction of leukemic differentiation by LSD1i, 6MP, and CER *in vivo* to estimate the feasibility of these drug combinations. Mathematical modeling efforts have provided insights into the optimization of therapies in various diseases including chronic myeloid leukemia (Tang et al., 2011). Here, our mathematical modeling approach considered two cell types: non-differentiated and differentiated cells. The former matures into the latter at a rate depending on the drug concentration through a mitosis-independent process (Figure 5A) (Busch et al., 2015). In our model, cells proliferate, differentiate, and die according to a continuous-time Markov branching process, where the lifetime of a cell follows an exponential distribution until it differentiates or dies and the number of descendants for large ancestor counts is normally distributed (Yakovlev and Yanev, 2010). We assumed that there was no de-differentiation from the differentiated to the undifferentiated cell population and the growth rate of differentiated cells was small. After estimating the relevant rates for both cell types, we found suitable agreement between the observed data and our simulations, suggesting that our modeling assumptions are acceptable (Figure S19). We then built a landscape for each rate parameter across a range of drug concentrations. Using published pharmacokinetic parameters for LSD1i and 6MP, we constructed compartmental models to predict the drug concentration in plasma for a multi-dose treatment schedule. Lastly, we combined the pharmacodynamic and pharmacokinetic models by using the predicted drug concentration at a given time from the pharmacokinetic model as an input to the pharmacodynamic model to predict the birth, differentiation, and death rates over time. This modeling generated time-dependent rates specific to each cell type and drug-combination regimen (Figure 5B).

Using the time-dependent rates from our model ensemble, we simulated two-week in silico trials by implementing our model for each specified regimen of LSD1i and 6MP. Since CER had the lowest stability in

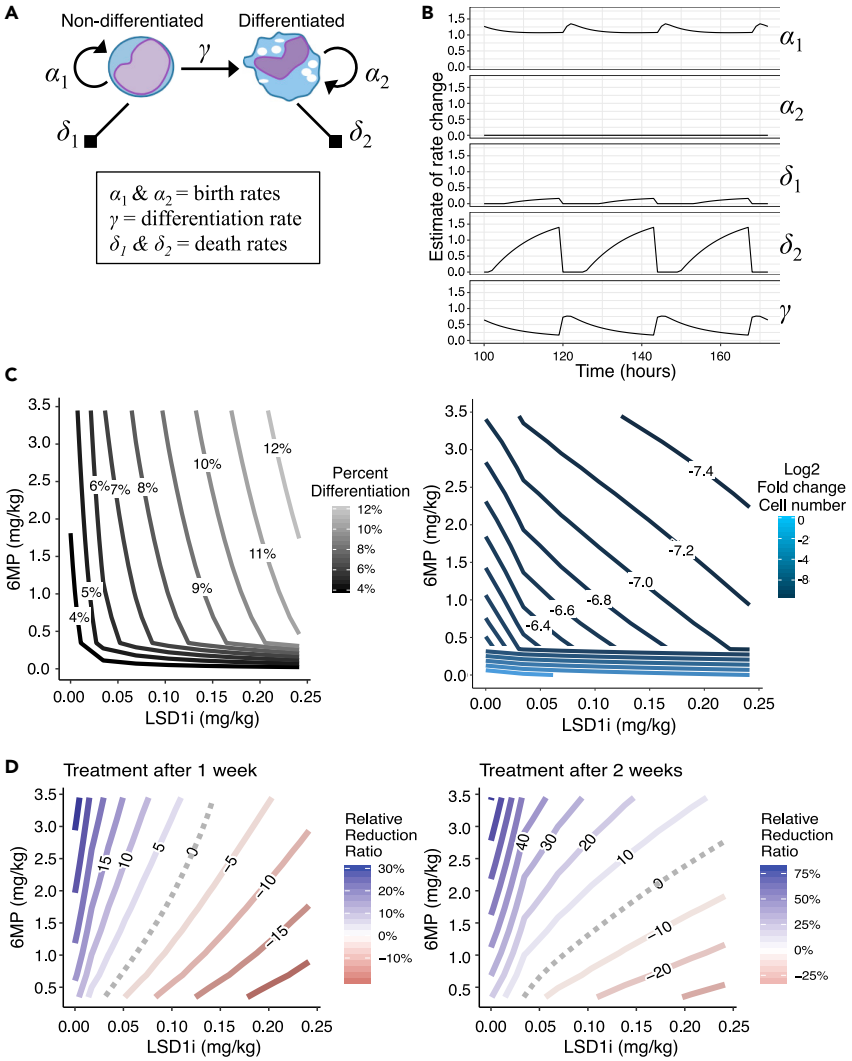

Figure 5. Optimal dosage schemes of LSD1i and 6MP administration to reduce tumor cell numbers

(A) Schematic model of tumor growth and differentiation. We consider 2 types of cells: non-differentiated and differentiated cells, that have their own birth rates termed α_1 and α_2 respectively and death rates termed δ_1 and δ_1, respectively. The parameter α_2 was set to a low value to represent the lack of self-renewal of differentiated cells. We assume that a cell can differentiate through a mitosis-independent process at a rate of γ.

(B) Change in rates of growth, differentiation, and death rates described in Panel A, where 0.5mg/kg LSD1i and 5mg/kg 6MP dose are given every twenty-four hours.

(C) Contour plot depicting the percentage of differentiated cells after 2 weeks of treatment (left) and the $\log_2$ fold change in total cell numbers after 2 weeks of the group treated with various doses of LSD1i and 6MP administered every twenty-four hours compared to the non-treated group (right). Color of lines represents levels of differentiation or fold change.

(D) Contour plot comparing two different drug schedules: treatment with 6MP daily and LSD1i every 48 hr or treatment with LSD1i daily and 6MP every 48 hr at the doses specified along the axes after one week (left) or two weeks (right) of treatment. The blue area represents doses where the former schedule would be more effective at decreasing the number of cells, whereas the red area represents doses where the latter schedule would be more effective. Color of lines represent the relative reduction ratio of the former schedule over the latter, where positive values indicate the former outperforms the latter. See also Figures S19–S22 and Table S17.

plasma (Figure S9C) and no murine pharmacokinetic model was available, we did not model the *in vivo* interactions of CER. At a given daily dose of LSD1i and 6MP, the prevalence of differentiated cells increased with both drugs, while the total tumor burden decreased with both drugs (Figure 5C). We then compared dose schedules that varied with respect to the intervals between doses (Figure 5D). Specifically, we compared two schedules: treatment with 6MP daily and LSD1i every 48 hr, or treatment with LSD1i daily

and 6MP every 48 hr at specified doses. At certain concentrations, one schedule outperformed the other after one or two weeks of treatment (Figure 5D): our model predicts that 0.5 mg/kg daily of LSD1 and 5 mg/kg of 6-MP every 48 hr would provide similar results after 2 weeks as 0.5 mg/kg of LSD1 every 48 hr and 5 mg/kg daily of 6-MP. Additionally, a drug holiday schedule of LSD1, with four days on and three days off, is predicted to fare better than administering LSD1 every 48 hr, regardless of the daily dose of 6-MP (Figure S20). The merits of our model's predictions would be bolstered by *in vivo* validation.

Proliferation and differentiation response to drugs in patient-derived AML specimens

We next tested whether LSD1i, 6MP, and CER induced a proliferation or differentiation response in primary human leukemia cells. We used two complementary systems: (1) patient-derived primary AML cells (PAMLs) directly transferred to tissue culture and 2) PAMLs that were transplanted and recovered from immune-compromised mice and subsequently transferred into tissue culture, which we termed as "patient-derived xenografts" or PDXs.

We treated four genetically distinct PAMLs (AML2741, AML2012, AML2920, and AML2928) with LSD1i, 6MP, and CER as single and as triple combinations (Duy et al., 2019) (Table S17). To assess differentiation, we monitored expression of CD11b and CD16 by flow cytometry (Figure S21A), as these cells lack the *Lyz2-GFP* reporter. All four PAMLs showed little to no growth sensitivity to CER treatment compared to vehicle treatment, but showed significant growth reduction in response to LSD1i, 6MP, and triple combination treatments ($p_{adj} < 1 \times 10^{-6}$) (Figure S21B). All four PAMLs showed significant differentiation following single treatment with LSD1i, and one PAML (AML2741) showed a further significant increase in differentiation following triple treatment compared to LSD1i alone (Figure S21C).

We next treated two PDXs, DFAM-15354 and DFAM-61345, which retain leukemic properties (including proliferation, HOXA9 expression, and CD34 expression) in the presence of either supporting stromal cells or conditioned media (Table S17). We found that both DFAM-61345 and DFAM-15354 showed significantly reduced proliferation when treated with the triple drug combination in stromal co-culture and conditioned media, respectively (Figures S22A and S22B). We next assayed the differentiation response of both PDXs after eight days of drug treatment by monitoring CD11b and CD16 as above. The percentage of differentiated cells significantly increased for both PDXs after single-drug treatment with LSD1i compared to vehicle, and differentiation was further increased by triple-drug treatment compared to LSD1i alone (Figure S22C). The response of a heterogeneous group of primary human leukemic cells, in two distinct systems, to triple drug treatment suggests that this may represent a promising therapeutic approach for AML.

DISCUSSION

Differentiation of hematopoietic stem cells to committed progenitors, and ultimately to mature cells, relies on appropriate regulation of transcription factors, cytokine receptor, and epigenetic factors. Mutations in the genes coding for these proteins are among the most common variants observed in patients with AML, and promote a stem-like state incapable of maturation (Tyner et al., 2018). The drugs in this study—LSD1i, 6MP, and CER—do not modify such mutations. Rather, we believe that the drug combinations promote a chromatin and metabolic states that allow cells to partially bypass the differentiation blockade. Our data suggest that the differentiation phenotype induced by the drug combinations arises through the known metabolic pathways of each individual drug, although how the pathways mechanistically interact with each other remain to be clarified. Previous studies have linked 6-thioguanine metabolism and lipid-regulatory gene expression with LSD1 activity, as well as the consumption of S-adenosylmethionine (SAM) during phosphatidylcholine formation with histone methylation (Ye et al., 2017) (Yuan et al., 2011) (Abdulla et al., 2014). Our report provides further evidence in support of a connection between the pathways targeted by LSD1i, 6MP, and CER in hematopoietic cells.

Our finding that 6MP metabolism via purine salvage promotes differentiation appears to complement recent findings that perturbation to *de novo* pyrimidine synthesis also promotes differentiation (Sykes et al., 2016). In considering a potential link between these findings, one hypothesis is that depletion of nucleotides, whether pyrimidine or purine, is sufficient to bypass the differentiation blockade. Although 6MP-derived metabolites can inhibit *de novo* purine synthesis (Tay et al., 1969), we do not believe this effect contributes significantly to differentiation, because neither mizoribine nor pentostatin, which deplete guanosine and inosine, respectively, promoted differentiation in our screen (Table S2). Additionally, ER-HOXA9 cells express low levels of *TPMT*, an enzyme required to process 6MP into an inhibitory metabolite.

In short, while a general demand of purines and pyrimidines for nucleic acid assembly may still be relevant for the AML differentiation blockade, we believe our 6MP findings speak more to the relevance of processes specific to 6MP.

We found that the triple combination of LSD1i, 6MP, and CER induced the greatest fraction of ER-HOXA9 cells to differentiate, at approximately 30–50% differentiation after 4 days of treatment depending on the clone (Figures S6 and S7). This treatment did not achieve the 70–80% differentiation induced by the novel dihydroorotate dehydrogenase inhibitor ML390 or the OMP decarboxylase inhibitor pyrazofurin as single agents (Sykes et al., 2016). Future investigations of the differentiation response induced by the triple combination across specific leukemia subtypes may identify genetic signatures that confer more sensitive responses.

Research into LSD1 inhibitors for AML therapy remains active across multiple laboratories. The assessment of tolerability of new LSD1 inhibitor compounds such as CC-90011 will motivate studies of whether such compounds can be safely and effectively paired with 6MP and CER (Maes et al., 2018) (Salamero et al., 2020) (Kanouni et al., 2020). Beyond these metabolic drugs though, it would be interesting to compare the efficiency of differentiation induction and proliferation reduction from treatment with the LSD1i, 6MP, and CER triple combination to other published epigenetic-based strategies. Examples of such strategies include combining LSD1 inhibitors with RAD001 (mTORC1 inhibitor), SYC-522 (DOT1L inhibitor), all-trans retinoic acid, and azacytidine, where the latter two combinations are currently being evaluated in clinical trials (Deb et al., 2020) (Feng et al., 2016) (Wass et al., 2020) (Buesa et al., 2019). As transcriptional programs are clarified in AML differentiation blockade, such as the IRX3-HOXA9 axis, and additional new pathways that cooperate with LSD1 inhibition are characterized, such studies may uncover the relative contributions, if any, of LSD1 catalytic activity and LSD1 interactions with binding partners such as GFI1 in bypassing the AML differentiation blockade in specific subtypes (Maiques-Diaz et al., 2018) (Somerville et al., 2018).

The modeling of human pharmacokinetic and pharmacodynamics responses to the drug combinations will be more complex than the murine *in silico* trials used here, given the differences in metabolism between humans compared to individual mice in isogenic strains. Although it is difficult to predict the feasibility of administrating these drug combinations for human clinical applications, these studies provide a starting point for targeting chromatin and metabolic pathways in the context of bypassing the AML differentiation blockade. Since the discovery of 6MP and CER in the 1950s and 1960s, respectively, both metabolic compounds have continued to be used by researchers in many contexts, including leukemia (Choi et al., 2015) (Aboul-Soud et al., 2016). Our findings have built upon this foundation of drug characterization as a means of acquiring biological insights into an important disease hallmark, and hopefully our findings will enable strategic and therapeutic innovations in AML management.

Limitations of study

This study used a diverse range of immortalized and primary cell lines to characterize the differentiation response induced by the triple combination of GSK-LSD1, 6-mercaptopurine, and cerulenin. Although morphological and molecular markers of mature myeloid cells suggest bona fide differentiation induced by the triple drug combination, features such as phagocytosis and loss of clonogenicity were not assayed. Additionally, it is not clear whether the triple drug combination in this study would be effective at inducing differentiation, reducing tumor burden, and extending survivability in animal models AML. Future studies that examine a broader panel of primary patient-derived cells may reveal the key genetic subtypes that confer the greatest differentiation sensitivity to these drugs and help identify the most genetically appropriate disease models.

STAR★METHODS

Detailed methods are provided in the online version of this paper and include the following:

- KEY RESOURCES TABLE
- RESOURCE AVAILABILITY
  - Lead contact
  - Materials availability
  - Data and code availability
- EXPERIMENTAL MODELS AND SUBJECT DETAILS

SUPPLEMENTAL INFORMATION

Supplemental information can be found online at https://doi.org/10.1016/j.isci.2021.102651.

ACKNOWLEDGMENTS

We thank Drs. Peggy Hsu, Brian Do, Haihua Chu, Haiming Xu, Laura Bond, Ellen Weisberg, Monica Reis, Scott Armstrong, Alejandro Gutierrez, David Williams, Kim Stegmaier, and Paresh Vyas for insightful discussions and comments. The primary screen was performed with the support of the ICCB-Longwood Screening Facility (Harvard Medical S chool). We thank Drs. Suzan Lazo and John Daley at the Dana Farber Flow Cytometry Core and Dr. Jen Smith at the ICCB-Longwood Screening facility for flow cytometry data acquisition. We thank Dr. Victoria Petkova of the Molecular Medicine Core (Beth Israel Deaconess Medical Center) for quality-control assessment of the RNA-seq samples. Nextseq support services were provided by the Boston Children's Hospital Intellectual and Developmental Disabilities Research Center Molecular Genetics Core Facility, which is supported by U54HD090255 from the NIH Eunice Kennedy Shriver National Institute of Child Health and Human Development. We thank GENEWIZ for ATAC-seq services. Cells were a gift from Drs. Martha Sola-Visner, Alejandro Gutierrez, James Griffin, Irene Ghobrial, William Kaelin, Dipak Panigrahy, Kathrin Bernt, Scott Armstrong, Kimberly Stegmaier, and Brian Liau. Y.S. acknowledges funding from BCH, Ludwig Institute for Cancer Research and the NIH (1R35CA210104-01). Y.S. is an American Cancer Society Research Professor. K.E.P. acknowledges funding from the Ludwig Center at Harvard. C.Y. acknowledges support from the AACR Anna D. Barker Basic Cancer Research Fellowship. G.W. is a fellow of the Leukemia and Lymphoma Society. A.J. acknowledges support from the Ludwig Center at Harvard. I.S. acknowledges funding from the Ludwig Center at Harvard Medical School, Breast Cancer Coalition of Rochester, Breast Cancer Research Foundation, and American Association for Cancer Research. F.M. acknowledges funding from the Dana-Farber Cancer Institute Physical Sciences-Oncology Center, grant number: NIH U54CA193461 and support from the Ludwig Center at Harvard. M.C.H. acknowledges funding from the NCI (R01CA213062). J.D.L. acknowledges funding from the Leukemia and Lymphoma Society Specialized Center of Research and the Samuel Waxman Cancer Research Foundation. D.M.W. acknowledges funding from the National Cancer Institute, grant number: NCI R35 CA231958-01A1.

AUTHOR CONTRIBUTIONS

Conceptualization, B.M.Z., A.D., J.M., A.J., M.A.B., Y.S.; Methodology, B.M.Z., K.E.P., C.Y., S.B.L., D.B.S.; Software, B.M.Z., K.E.P.; Validation, B.M.Z.; Formal Analysis, B.M.Z., K.E.P.; Investigation, B.M.Z., K.E.P., C.-H.Y., K.C.K., G.W., W.D.J., E.S., A.D.; Resources, C.D., J.E.E., I.S.H., D.B.S.; Data Curation, B.M.Z.; Writing – Original Draft, B.M.Z., K.E.P., C.-H.Y; Writing – Review & Editing: K.C.K., G.W., C.D., W.D.J., E.S., J.E.E., A.J., S.B.L., J.M., A.D., I.S.H., M.A.B., D.B.S., J.D.L., D.M.W., A.M., M.C.H., F.M. Y.S.; Visualization, B.M.Z., K.E.P.; Supervision, D.M.W., A.M., M.C.H, F.M., Y.S.; Project Administration, Y.S.; Funding Acquisition, Y.S.

DECLARATION OF INTERESTS

Y.S. is a co-founder and equity holder of Constellation Pharmaceuticals, Athelas Therapeutics and K36 Therapeutics, a consultant for Active Motif, and an equity holder of Imago Biosciences. I.S.H. is a consultant

for ONO Pharma USA. D.B.S. is a co-founder and an equity holder of Clear Creek Bio. Y.S., B.M.Z, J.M., and A.D. are developers of the LSD1 inhibitor combinations described in this report and Boston Children's Hospital has pursued a patent application of this technology. All other authors declare no competing financial interests.

Received: August 24, 2020
Revised: December 3, 2020
Accepted: May 24, 2021
Published: June 25, 2021

REFERENCES

Abdel-Aziz, A.K., and Minucci, S. (2019). Comparing apples with oranges: studying LSD1 inhibitors in cellular assays. Pharmacol. Res. *146*, 104345.

Abdulla, A., Zhang, Y., Hsu, F.N., Xiaoli, A.M., Zhao, X., Yang, E.S.T., Ji, J.Y., and Yang, F. (2014). Regulation of lipogenic gene expression by lysine-specific histone demethylase-1 (LSD1). J. Biol. Chem. *289*, 29937–29947.

Aboul-Soud, M.A.M., El-Shemy, H.A., Aboul-Enein, K.M., Mahmoud, A.M., Al-Abd, A.M., and Lightfoot, D.A. (2016). Effects of plant-derived anti-leukemic drugs on individualized leukemic cell population profiles in Egyptian patients. Oncol. Lett. *11*, 642–648.

Bohon, J., and de los Santos, C.R. (2005). Effect of 6-thioguanine on the stability of duplex DNA. Nucleic Acids Res. *33*, 2880–2886.

Bräutigam, L., Zhang, J., Dreij, K., Spahiu, L., Holmgren, A., Abe, H., Tew, K.D., Townsend, D.M., Kelner, M.J., Morgenstern, R., et al. (2018). MGST1, a GSH transferase/peroxidase essential for development and hematopoietic stem cell differentiation. Redox Biol. *17*, 171–179.

Buesa, C., Somervaille, T.C.P., Arevalo, M., Xaus, J., Gutierrez, S., and Bullock, R. (2019). Iadademstat shows efficacy in elerly AML patients in combination with azacitidine alice trial. Blood *134*, 3839.

Burns, C.P. (1975). Isoleucine metabolism by leukemic and normal human leukocytes in relation to cell maturity and type. Blood *45*, 643–651.

Busch, K., Klapproth, K., Barile, M., Flossdorf, M., Holland-Letz, T., Schlenner, S.M., Reth, M., Hofer, T., and Rodewald, H.R. (2015). Fundamental properties of unperturbed haematopoiesis from stem cells in vivo. Nature *518*, 542–546.

Choi, Y.W., Jeong, S.H., Ahn, M.S., Lee, H.W., Kang, S.Y., Choi, J.H., and Park, J.S. (2015). Oral maintenance chemotherapy with 6-mercaptopurine and methotrexate in patients with acute myeloid leukemia ineligible for transplantation. J. Korean Med. Sci. *30*, 1416–1422.

Chou, J., Chan, M.F., and Werb, Z. (2016). Metalloproteinases: a functional pathway for myeloid cells. Microbiol. Spect *4*, 10–1128.

Collins, C., Wang, J., Miao, H., Bronstein, J., Nawer, H., Xu, T., Figueroa, M., Muntean, A.G., and Hess, J.L. (2014). C/EBPα is an essential collaborator in Hoxa9/Meis1-mediated leukemogenesis. Proc. Natl. Acad. Sci. U S A *111*, 9899–9904.

Cusan, M., Cai, S.F., Mohammad, H.P., Krivtsov, A., Chramiec, A., Loizou, E., Witkin, M.D., Smitheman, K.N., Tenen, D.G., Ye, M., et al. (2018). LSD1 inhibition exerts its antileukemic effect by recommissioning PU.1- and C/EBPα-dependent enhancers in AML. Blood *131*, 1730–1742.

de Thé, H. (2018). Differentiation therapy revisited. Nat. Rev. Cancer *18*, 117–127.

Deb, G., Wingelhofer, B., Amaral, F.M.R., Maiques-Diaz, A., Chadwick, J.A., Spencer, G.J., Williams, E.L., Leong, H.S., Maes, T., and Somervaille, T.C.P. (2020). Pre-clinical activity of combined LSD1 and mTORC1 inhibition in MLL-translocated acute myeloid leukemia. Leukemia *34*, 1266–1277.

Demidenko, E., and Miller, T.W. (2019). Statistical determination of synergy based on Bliss definition of drugs independence. PLoS One *14*, e0224137.

Dobin, A., Davis, C.A., Schlesinger, F., Drenkow, J., Zaleski, C., Jha, S., Batut, P., Chaisson, M., and Gingeras, T.R. (2013). STAR: ultrafast universal RNA-seq aligner. Bioinformatics *29*, 15–21.

Döhner, H., Estey, E.H., Amadori, S., Appelbaum, F.R., Büchner, T., Burnett, A.K., Dombret, H., Fenaux, P., Grimwade, D., Larson, R.A., et al. (2010). Diagnosis and management of acute myeloid leukemia in adults: recommendations from an international expert panel, on behalf of the European LeukemiaNet. Blood *115*, 453–474.

Duy, C., Teater, M., Garrett-Bakelman, F.E., Lee, T.C., Meydan, C., Glass, J.L., Li, M., Hellmuth, J.C., Mohammad, H.P., Smitheman, K.N., et al. (2019). Rational targeting of cooperating layers of the epigenome yields enhanced therapeutic efficacy against AML. Cancer Discov. *9*, 872–889.

Elion, G.B., Singer, S., and Hitchings, G.H. (1953). The purine metabolism of a 6-mercaptopurine-resistant Lactobacillus casei. J. Biol. Chem. *204*, 35–41.

Faber, J., Krivtsov, A.V., Stubbs, M.C., Wright, R., Davis, T.N., van den Heuvel-Eibrink, M., Zwaan, C.M., Kung, A.L., and Armstrong, S.A. (2009). HOXA9 is required for survival in human MLL-rearranged acute leukemias. Blood *113*, 2375–2385.

Faust, N., Varas, F., Kelly, L.M., Heck, S., and Graf, T. (2000). Insertion of enhanced green fluorescent protein into the lysozyme gene creates mice with green fluorescent granulocytes and macrophages. Blood *92*, 719–726.

Feng, Z., Yao, Y., Zhou, C., Chen, F., Wu, F., Wei, L., Liu, W., Dong, S., Redell, M., Mo, Q., and Song, Y. (2016). Pharmacological inhibition of LSD1 for the treatment of MLL-rearranged leukemia. J. Hematol. Oncol. *9*, 24.

Gao, L., Sun, J., Liu, F., Zhang, H., and Ma, Y. (2016). Higher expression levels of the HOXA9 gene, closely associated with MLL-PTD and EZH2 mutations, predict inferior outcome in acute myeloid leukemia. Onco Targets Ther. *9*, 711–722.

Goldberg, I., Walker, J.R., and Bloch, K. (1973). Inhibition of lipid synthesis in Escherichia coli cells by the antibiotic cerulenin. Antimicrob. Agents Chemother. *3*, 549–554.

Harriman, G., Greenwood, J., Bhat, S., Huang, X., Wang, R., Paul, D., Tong, L., Saha, A.K., Westlin, W.F., Kapeller, R., et al. (2016). Acetyl-CoA carboxylase inhibition by ND-630 reduces hepatic steatosis, improves insulin sensitivity, and modulates dyslipidemia in rats. Proc. Natl. Acad. Sci. U S A *113*, E1796–E1805.

Harris, W.J., Huang, X., Lynch, J.T., Spencer, G.J., Hitchin, J.R., Li, Y., Ciceri, F., Blaser, J.G., Greystoke, B.F., Jordan, A.M., et al. (2012). The histone demethylase KDM1A sustains the oncogenic potential of MLL-AF9 leukemia stem cells. Cancer Cell *21*, 473–487.

Harris, I.S., Endress, J.E., Coloff, J.L., Selfors, L.M., McBrayer, S.K., Rosenbluth, J.M., Takahashi, N., Dhakal, S., Koduri, V., Oser, M.G., et al. (2019). Deubiquitinases maintain protein homeostasis and survival of cancer cells upon glutathione depletion. Cell Metab. *29*, 1166–1181.

Hastie, T.J. (1992). Generalized Additive Models in Statistical Models in S. 249–307 (CRC Press).

Juliusson, G. (2011). Older patients with acute myeloid leukemia benefit from intensive chemotherapy: an update from the Swedish Acute Leukemia Registry. Clin. Lymphoma Myeloma Leuk. *11*, S54–S59.

Kalin, J.H., Wu, M., Gomez, A.V., Song, Y., Das, J., Hayward, D., Adejola, N., Wu, M., Panova, I., Chung, H.J., et al. (2018). Targeting the CoREST complex with dual histone deacetylase and demethylase inhibitors. Nat. Commun. *9*, 53.

Kanouni, T., Severin, C., Cho, R.W., Yuen, N.Y.Y., Xu, J., Shi, L., Lai, C., Del Rosario, J.R., Stansfield, R.K., Lawton, L.N., et al. (2020). Discovery of CC-

90011: a potent and selective reversible inhibitor of lysine specific demethylase 1 (LSD1). J. Med. Chem. *63*, 14522–14529.

Kerenyi, M.A., Shao, Z., Hsu, Y.J., Guo, G., Luc, S., O'Brien, K., Fujiwara, Y., Peng, C., Nguyen, M., and Orkin, S.H. (2013). Histone demethylase Lsd1 represses hematopoietic stem and progenitor cell signatures during blood cell maturation. Elife *2*, e00633.

Kawabata, K.C., Zong, H., Meydan, C., Wyman, S., Wouters, B.J., Sugita, M., Goswami, S., Albert, M., Yip, W., Roboz, G.J., et al. (2021). BCL6 maintains survival and self-renewal of primary human acute myeloid leukemia cells. Blood *137*, 812–825.

Klés, V., Hyrien, O., Poul, J.M., and Sanders, P. (2003). Application of pharmacokinetic/pharmacodynamics and stochastic modelling to 6-mercaptopurine micronucleus induction in mouse bone marrow erythrocytes. J. Appl. Toxicol. *23*, 59–70.

Kreitz, J., Schönfeld, C., Seibert, M., Stolp, V., Alshamleh, I., Oellerich, T., Steffen, B., Schwalbe, H., Schnütgen, F., Kurrle, N., et al. (2019). Metabolic plasticity of acute myeloid leukemia. Cells *8*, E805.

Krystosek, A., and Sachs, L. (1976). Control of lysozyme induction in the differentiation of myeloid leukemic cells. Cell *9*, 675–684.

Lee, J.S., Mendez, R., Heng, H.H., Yang, Z.Q., and Zhang, K. (2012). Pharmacological ER stress promotes hepatic lipogenesis and lipid droplet formation. Am. J. Transl. Res. *4*, 102–113.

Lennard, L. (1992). The clinical pharmacology of 6-mercaptopurine. Eur. J. Clin. Pharmacol. *43*, 329–339.

Leyssen, P., Balzarini, J., De Clercq, E., and Neyts, J. (2005). The predominant mechanism by which ribavirin exerts its antiviral activity in vitro against flaviviruses and paramyxoviruses is mediated by inhibition of IMP dehydrogenase. J. Virol. *79*, 1943–1947.

Maes, T., Mascaró, C., Tirapu, I., Estiarte, A., Ciceri, F., Lunardi, S., Guibourt, N., Perdones, A., Lufino, M.M.P., Somervaille, T.C.P., et al. (2018). ORY-1001, a potent and selective covalent KDM1A inhibitor, for the treatment of acute leukemia. Cancer Cell *33*, 495–511.

Maiques-Diaz, A., Lynch, J.T., Spencer, G.J., and Somervaille, T.C.P. (2018). LSD1 inhibitors disrupt the GFI1 transcription repressor complex. Mol. Cell. Oncol. *5*, e1481813.

McCune, S.A., and Harris, R.A. (1979). Mechanism responsible for 5-(tetradecyloxy)-2-furoic acid inhibition of hepatic lipogenesis. J. Biol. Chem. *254*, 10095–10101.

McGrath, J.P., Williamson, K.E., Balasubramanian, S., Odate, S., Arora, S., Hatton, C., Edwards, T.M., O'Brien, T., Magnuson, S., Stokoe, D., et al. (2016). Pharmacological inhibition of the histone lysine demethylase KDM1A suppresses the growth of multiple acute myeloid leukemia subtypes. Cancer Res. *76*, 1975–1988.

Mohammad, H.P., Smitheman, K.N., Kamat, C.D., Soong, D., Federowicz, K.E., Van Aller, G.S., Schneck, J.L., Carson, J.D., Liu, Y., Butticello, M., et al. (2015). A DNA hypomethylation signature predicts antitumor activity of LSD1 inhibitors in SCLC. Cancer Cell *28*, 57–69.

Neese, R.A., Misell, L.M., Turner, S., Chu, A., Kim, J., Cesar, D., Hoh, R., Antelo, F., Strawford, A., McCune, J.M., et al. (2002). Measurement in vivo of proliferation rates of slow turnover cells by $^{2}H_{2}O$ labeling of the deoxyribose moiety of DNA. Proc. Natl. Acad. Sci. U S A *99*, 15345–15350.

Nomura, S., Horiuchi, T., Omura, S., and Hata, T. (1972). The action mechanism of cerulenin. I. Effect of cerulenin on sterol and fatty acid biosynthesis in yeast. J. Biochem. *71*, 783–796.

Ramírez, F., Ryan, D.P., Grüning, B., Bhardwaj, V., Kilpert, F., Richter, A.S., Heyne, S., Dündar, F., and Manke, T. (2016). deepTools2: a next generation web server for deep-sequencing data analysis. Nucleic Acids Res. *44*, W160–W165.

Roney, J.P., Ferlic, J., Michor, F., and McDonald, T.O. (2020). ESTIpop: a computational tool to simulate and estimate parameters for continuous-time Markov branching processes. Bioinformatics *36*, 4372–4373.

Salamero, O., Montesinos, P., Willekens, C., Pérez-Simón, J.A., Pigneux, A., Récher, C., Popat, R., Carpio, C., Molinero, C., Mascaró, C., et al. (2020). First-in-human phase I study of iadademstat (ORY-1001): a first-in-class lysine-specific histone demethylase 1a inhibitor, in relaped or refractory acute myeloid leukemia. J. Clin. Oncol. *38*, 4260–4273.

Schenk, T., Chen, W.C., Gollner, S., Howell, L., Jin, L., Hebestreit, K., Klein, H.U., Popescu, A.C., Burnett, A., Mills, K., et al. (2012). Inhibition of the LSD1 (KDM1A) demethylase reactivates the all-trans-retinoic acid differentiation pathway in acute myeloid leukemia. Nat. Med. *18*, 605–611.

Schmidt, D.M., and McCafferty, D.G. (2007). trans-2-Phenylcyclopropylamine is a mechanism-based inactivator of the histone demethylase LSD1. Biochemistry *46*, 4408–4416.

Scholar, E.M., Brown, P.R., and Parks, R.E., Jr. (1972). Synergistic effect of 6-mercaptopurine and 6-methylmercaptopurine ribonucleoside on the levels of adenine nucleotides of Sarcoma 180 cells. Cancer Res. *32*, 259–269.

Somerville, T.D.D., Simeoni, F., Chadwick, J.A., Williams, E.L., Spencer, G.J., Boros, K., Wirth, C., Tholouli, E., Byers, R.J., and Somervaille, T.C.P. (2018). Derepression of the Iroquois homeodomain transcription factor gene IRX3 confers differentiation block in acute leukemia. Cell Rep. *22*, 638–652.

Sykes, D.B., Kfoury, Y.S., Mercier, F.E., Wawer, M.J., Law, J.M., Haynes, M.K., Lewis, T.A., Schajnovitz, A., Jain, E., Lee, D., et al. (2016). Inhibition of dihydroorotate dehydrogenase overcomes differentiation blockade in acute myeloid leukemia. Cell *167*, 171–186.

Tang, M., Gonen, M., Quintas-Cardama, A., Cortes, J., Kantarjian, H., Field, C., Hughes, T.P., Branford, S., and Michor, F. (2011). Dynamics of chronic myeloid leukemia response to long-term targeted therapy reveal treatment effects on leukemic stem cells. Blood *118*, 1622–1631.

Tay, B.S., Lilley, R.M., Murray, A.W., and Atkinson, M.R. (1969). Inhibition of phosphoribosyl pyrophosphate amidotransferase from Ehrlich ascites-tumour cells by thiopurine nucleotides. Biochem. Pharmacol. *18*, 936–938.

Thomas, X., and Le Jeune, C. (2017). Treatment of elderly patients with acute myeloid leukemia. Curr. Treat. Options Oncol. *18*, 2.

Thupari, J.N., Pinn, M.L., and Kuhajda, F.P. (2001). Fatty acid synthase inhibition in human breast cancer cells leads to malonyl-CoA-induced inhibition of fatty acid oxidation and cytotoxicity. Biochem. Biophys. Res. Commun. *285*, 217–223.

Townsend, E.C., Murakami, M.A., Christodoulou, A., Christie, A.L., Koster, J., DeSouza, T.A., Morgan, E.A., Kallgren, S.P., Liu, H., Wu, S.C., et al. (2016). The Public Repository of Xenografts enables discovery and randomized Phase II-like trials in mice. Cancer Cell *29*, 574–586.

Tyner, J.W., Tognon, C.E., Bottomly, D., Wilmot, B., Kurtz, S.E., Savage, S.L., Long, N., Schult, A.R., Traer, E., Abel, M., et al. (2018). Functional genomic landscape of acute myeloid leukemia. Nature *562*, 526–531.

Visram, M., Radulovic, M., Steiner, S., Malanovic, N., Eichmann, T.O., Wolinski, H., Rechberger, G.N., and Tehlivets, O. (2018). Homocysteine regulates fatty acid and lipid metabolism in yeast. J. Biol. Chem. *293*, 5544–5555.

Vlodavsky, I., Fibach, E., and Sachs, L. (1975). Control of normal differentiation of myeloid leukemic cells. X. Glucose utilization, cellular ATP and associated membrane changes in D+ and D- cells. J. Cell Physiol. *87*, 167–177.

Wang, G.G., Calvo, K.R., Pasillas, M.P., Sykes, D.B., Hacker, H., and Kamps, M.P. (2006). Quantitative production of macrophages or neutrophils ex vivo using conditional Hoxb8. Nat. Methods *3*, 287–293.

Ward, J.L., Sherali, A., Mo, Z.P., and Tse, C.M. (2000). Kinetic and pharmacological properties of cloned human equilibrative nucleoside transporters, ENT1 and ENT2, stably expressed in nucleoside transporter-deficient PK15 cells. Ent2 exhibits a low affinity for guanosine and cytidine but a high affinity for inosine. J. Biol. Chem. *275*, 8375–8381.

Wass, M., Göllner, S., Besenbeck, B., Schlenk, R.E., Mundmann, P., Göthert, J.R., Noppeney, R., Schliemann, C., Mikesch, J.H., Lenz, G., et al. (2020). A proof of concept phase I/II pilot trial of LSD1 inhibition by tranylcypromine combined with ATRA in refractory/relapsed AML patients no eligible for intensive therapy. Leukemia *19*, 1–11.

Weber, M.J., and Rubin, H. (1971). Uridine transport and RNA synthesis in growing and in density-inhibited animal cells. J. Cell Physiol. *77*, 157–168.

Werstuck, G.H., Lentz, S.R., Dayal, S., Hossain, G.S., Sood, S.K., Shi, Y.Y., Zhou, J., Maeda, N., Krisans, S.K., Malinow, M.R., et al. (2001). Homocysteine-induced endoplasmic reticulum stress causes dysregulation of the cholesterol and triglyceride biosynthetic pathways. J. Clin. Invest. *107*, 1263–1273.

Wishart, D.S., Feunang, Y.D., Marcu, A., Guo, A.C., Liang, K., Vazquez-Fresno, R., Sajed, T., Johnson, D., Li, C., Karu, N., et al. (2018). Hmdb 4.0: the human metabolome database for 2018. Nucleic Acid Res. *46*, D608–D617.

Yakovlev, A.Y., and Yanev, N.M. (2010). Limiting distributions for multitype branching processes. Stoc. Anal. Appl. *28*, 1040–1060.

Yao, C.H., Wang, L., Stancliffe, E., Sindelar, M., Cho, K., Weitong, Y., Wang, Y., and Patti, G.J. (2020). Dose-response metabolomics to understand biochemical mechanisms and off-target drug effects with the TOXcms software. Anal. Chem. *92*, 1856–1864.

Ye, C., Sutter, B.M., Wang, Y., Kuang, Z., and Tu, B.P. (2017). A metabolic function for phospholipid and histone methylation. Mol. Cell. *66*, 180–193.

Yuan, B., and Wang, Y. (2008). Mutagenic and cytotoxic properties of 6-thioguanine, S6-methylthioguanine, and guanine-S6-sulfonic acid. J. Biol. Chem. *283*, 23665–23670.

Yuan, B., Zhang, J., Wang, H., Xiong, L., Cai, Q., Wang, T., Jacobsen, S., Pradhan, S., and Wang, Y. (2011). 6-Thioguanine reactivates epigenetically silenced genes in acute lymphoblastic leukemia cells by facilitating proteasome-mediated degradation of DNMT1. Cancer Res. *71*, 1904–1911.

STAR★METHODS

KEY RESOURCES TABLE

REAGENT or RESOURCE	SOURCE	IDENTIFIER
Antibodies		
APC-CD11b	BioLegend	Cat# 101212; RRID:AB_312795
Pacific Blue-CD45	BioLegend	Cat# 304022; RRID:AB_493655
FITC-CD16	BioLegend	Cat# 302006; RRID:AB_314206
Chemicals, peptides, and recombinant proteins		
$^{13}C_5$-hypoxanthine	Cambridge Isotope Laboratories	CLM-8042
2′-deoxy-6-thioguanosine	Carbosynth	ND08563
6-thioguanine	Cayman Chemical	15774
6-thioguanosine	Carbosynth	NT04480
Beta-estradiol	Sigma Aldrich	E4389
BIT 9500	Fisher Scientific	NC9952276
Cerulenin	Cayman Chemical	10005647
Cytarabine	Sigma Aldrich	PHR1787
Dimethyl sulfoxide	Sigma Aldrich	D8418
DNA Degradase Plus	Zymo Research	E2020
FLT3L	Peprotech	10773-614
GSK-LSD1	Selleck	S7574
Guanosine	Cayman Chemical	27702
Homocysteine	Sigma Aldrich	H4628
Hypoxanthine	Sigma Aldrich	H9636
IL-3	Stemcell technologies	78040
IL-6	Peprotech	200-06
Mercaptopurine	Tocris	4103
ND-630	MedChemExpress	HY-16901
P1 Nuclease	New England Biolabs	M0660S
Penicillin-Streptomycin	Corning	30002CI
Propidium iodide	Invitrogen	P3566
SCF	Peprotech	300-07
Shrimp Alkaline Phosphatase	New England Biolabs	M0371S
TOFA	MedChemExpress	HY-101068
TPO	Peprotech	300-18
Tranylcypromine	Sigma Aldrich	P8511
Trizol	ThermoFisher	15596018
Deposited data		
Flow cytometry and MRM dataset	Zee, Barry (2021), "LMC-FlowCytometry-MRM", Mendeley Data, V2, https://doi.org/10.17632/h87tr4kw4f.2 https://data.mendeley.com/datasets/h87tr4kw4f/1	
Metabolomics Part 1 and microscopy	Zee, Barry (2021), "LMC-Metabolomics-RPLCpos-original-microscopyimages", Mendeley Data, V2, https://doi.org/10.17632/xh7mxz69mz.2 https://data.mendeley.com/datasets/xh7mxz69mz/1	
Metabolomics Part 2	Zee, Barry (2021), "LMC-Metabolomics-HILIC-RPLCneg", Mendeley Data, V2, https://doi.org/10.17632/bgfxnmr58c.2 https://data.mendeley.com/datasets/bgfxnmr58c/1	
ATAC-seq and RNA-seq	GSE162398	

(*Continued on next page*)

Continued

REAGENT or RESOURCE	SOURCE	IDENTIFIER
Experimental models: cell lines		
CCRF-CEM (human)	Boston Children's Hospital	N/A
Cord CD34+ (human)	Boston Children's Hospital	N/A
DFAM-15354 (human)	Dana Farber Cancer Institute	N/A
DFAM-61345 (human)	Dana Farber Cancer Institute	N/A
EL4 (mouse)	Beth Israel Deaconess Medical Center	PMID: 29191914
ER-HOXA9 (mouse)	Massachusetts General Hospital	PMID: 27641501
ER-HOXB8 (mouse)	Massachusetts General Hospital	PMID: 16554834
HOXA9:MEIS1 (mouse)	Massachusetts General Hospital	PMID: 27641501
HS-5 (human)	Dana Farber Cancer Institute	N/A
HS27 (human)	American Type Culture Collection	CRL-1634
Jurkat (human)	Boston Children's Hospital	N/A
K562 (human)	Boston Children's Hospital	N/A
MN1 (mouse)	Children's Hospital of Philadelphia	PMID: 26927674
MOLM13 (human)	Dana Farber Cancer Institute	N/A
MOLM14 (human)	Dana Farber Cancer Institute	N/A
MOLT4 (human)	Boston Children's Hospital	N/A
MV4,11 (human)	Harvard University	N/A
NOMO1 (human)	Dana Farber Cancer Institute	N/A
OCI-AML2 (human)	Dana Farber Cancer Institute	N/A
PF382	Boston Children's Hospital	N/A
SKM-1 (human)	Dana Farber Cancer Institute	N/A
TF-1 (human)	Dana Farber Cancer Institute	PMID: 23393090
THP1 (human)	Dana Farber Cancer Institute	N/A
U937 (human)	Boston Children's Hospital	N/A
Oligonucleotides		
See Table S18 for full list of primers	ThermoFisher	This study
Software and algorithms		
Estipop	https://github.com/Michorlab/AML_scheduleOptimization	
Rstatix	https://cran.r-project.org/web/packages/rstatix/index.html	
Tidyverse	https://cran.r-project.org/web/packages/tidyverse/index.html	

RESOURCE AVAILABILITY

Lead contact

Further information and requests for resources and reagents should be directed to and will be fulfilled by the lead contact, Yang Shi (Yang.Shi@childrens.harvard.edu and yang.shi@ludwig.ox.ac.uk)

Materials availability

This study did not generate new unique reagents.

Data and code availability

Data and code are available at Mendeley at the following links:

Flow cytometry and MRM dataset: https://data.mendeley.com/datasets/h87tr4kw4f/1, Metabolomics Part 1 and microscopy: https://data.mendeley.com/datasets/xh7mxz69mz/1, Metabolomics Part 2: https://data.mendeley.com/datasets/bgfxnmr58c/1.

ATAC-seq and RNA-seq data are available at Gene expression omnibus (GEO GSE162398), and Github (https://github.com/Michorlab/AML_scheduleOptimization). All other data are available upon request.

EXPERIMENTAL MODELS AND SUBJECT DETAILS

Tissue culture

ER-HOXA9 and ER-HOXB8 cells were passaged as described, in RPMI-1640 media (Invitrogen) supplemented with 10% volume heat-inactivated fetal bovine serum (Gemini Bio), stem cell factor (SCF, derived from conditioned media), 4mM glutamine (Corning), and 0.5μM beta-estradiol (Sigma Aldrich) (Sykes et al., 2016). HOXA9-MEIS1 cells were similarly passaged as ER-HOXA9 cells except without E2. Umbilical cord derived CD34 + cells were passaged in StemSpan (Stemcell Technologies) media with 10ng/ml each of GM-CSF, TPO, SCF1, and IL3. TF-1 cells were passaged in RPMI-1640 with HS-5 conditioned media.

For primary AML studies, cells had been provided as cryopreserved specimens, and maintained as previously described (Kawabata et al., 2021) (Duy et al., 2019). Briefly, PAML cells were maintained in IMDM tissue culture medium supplemented with 20%FCS, 20% BIT (BSA-Insulin-Transferrin, Fisher Scientific), 2-ME, and human IL-3, IL-6, G-CSF, GM-CSF, SCF, and FLT3-Ligand (STEMCELL Technologies). *Ex vivo* drug treatments were performed in triplicates using primary AML cells grown in 96-well plates. Those specimens were subjected to analysis using flow cytometry to detect cell viability with Zombie green, leukemia blast cells with CD45, and myeloid differentiation with CD16 and CD11b expression.

For patient-derived xenograft studies, HS27 (CRL-1634) stromal cells were obtained from ATCC and cultured in DMEM (Life Technologies) with 15% FBS (Sigma Aldrich) supplemented with 1% penicillin-streptomycin (Corning). PDX models DFAM-15354 and DFAM-61345 were generated as published (Townsend et al., 2016) and are publicly available from the DFCI Center for Patient-Derived Models (https://www.dana-farber.org/research/departments-centers-and-labs/integrative-research-centers/center-for-patient-derived-models/ordering-patient-derived-models/). HS27 cells were irradiated with 3500 cGy 48 hr before starting PDX AML cells co-culture. Irradiated HS27 cells were cultured for 48 hr and the supernatants were filtered through 0.25 um PVDF membrane and collected as conditional media. Primary PDX AML cells (from spleen) cryopreserved in 10% DMSO were quickly thawed and resuspended in 10 mL of RPMI-1640 (Life Technologies) with 20% FBS and centrifuged at 600 g for 5 min. Cells were then resuspended in conditional media supplemented with 50 uM β-mercaptoethanol and human cytokines including FLT3L (10 ng/mL; Peprotech), IL3 (10 ng/mL; STEMCELL Technologies, 78,040), IL6 (20 ng/mL; Peprotech), SCF (100 ng/mL; Peprotech) and TPO (10 ng/mL; Peprotech), and then plated on confluent irradiated HS27 cells in a 24-well plate.

All other lines were passaged in RPMI-1640 formulation as described above without any cytokines. All cells were grown in a 37°C humidified incubator with 5% CO_2.

METHOD DETAILS

Chemical screen

ER-HOXA9 cells were prepared in media with 50nM GSK-LSD1 (Selleck Chemical) and seeded at a density of 5×10^4 cells/ml in 200μL volume per well of a flat-bottom 96-well plastic plate (Genesee Scientific) using a Combi Reagent Dispenser (ThermoFisher). Drugs in 100% DMSO (Sigma Aldrich) were pin-transferred (V&P Scientific) from 384-well stock plates into the 96-well plates containing our cells at approximately 300nL drug stock per well (Table S1). The drug library was prepared as described in a previous report (Harris et al., 2019). Cells treated with GSK-LSD1 alone served as negative control, while cells treated with GSK-LSD1 and 100nM cytarabine (Sigma Aldrich), a known synergistic combination, served as a positive contorl (McGrath et al., 2016). Plates were incubated for 5 days and analyzed on an iQue Screener Plus-VBR flow cytometer (Intellicyt) running the Forecyt acquisition and analysis software. The overall gating strategy was (i) to isolate total cells using forward scatter (FSC) and side scatter (SSC) channels, (ii) to isolate live cells using the same aforementioned channels from total cells, and (iii) to isolate the differentiating Lyz2-GFP + cells using the blue laser channel (488nm excitation and 530nm emission). Viability was calculated by dividing the number of live cells by the number of total cells, and differentiation was calculated by dividing the number of Lyz2-GFP + cells by the number of live cells. The GFP + gate was set such that the negative control wells provided a differentiation percentage of ~3–5%. Drug combinations that lead to a differentiation percentage equal to or greater than the positive control (~19%) were considered potential hits.

In vitro drug treatment and flow cytometry

For non-screen drug plating, 2.5–5×10^3 live cells were seeded onto flat-bottom 96-well plastic plates in 200 μL of media per well. Drugs were added such that the total DMSO (Sigma-Aldrich) concentration was the same for all wells. After treatment, plates were transferred onto round-bottom 96-well plastic plates (Greiner Bio-One). Cells were analyzed on an iQue Screener Plus-VBR flow cytometer with a similar gating strategy as the one used for the screen, except we isolated singlets using both height and area parameters for FSC and SSC from live cells. We then isolated GFP + or antibody-positive events from the live singlets. GSK-LSD1, mercaptopurine (Tocris), cerulenin (Cayman Chemical), 6-thioguanine (Cayman Chemical), guanosine (Cayman Chemical), TOFA (MedChemExpress), ND-630 (MedChemExpress), hypoxanthine (Sigma Aldrich), and $^{13}C_5$-hypoxanthine (Cambridge Isotope Laboratories) were dissolved in DMSO as 10mM stocks. Tranylcypromine (Sigma Aldrich) and homocysteine (Sigma Aldrich) were dissolved in ethanol and water respectively as 100mM stock. APC-CD11b antibody (BioLegend) and propidium iodide (ThermoFisher) were used at concentrations of 1 μg/mL or 50 μg/mL respectively.

Genomic analyses

For ATAC-seq, ER-HOXA9 cells were treated with DNase before being washed with PBS and frozen with liquid nitrogen for processing by Genewiz. ATAC-seq library preparation and sequencing reactions were conducted at GENEWIZ, LLC. (South Plainfield, NJ, USA). Live cell samples were thawed, washed, and treated with DNAse I (Life Tech, Cat. #EN0521) to remove genomic DNA contamination. Live cell samples were quantified and assessed for viability using a Countess Automated Cell Counter (ThermoFisher Scientific). After cell lysis and cytosol removal, nuclei were treated with Tn5 enzyme (Illumina, Cat. #20034197) for 30 min at 37°C and purified with Minelute PCR Purification Kit (Qiagen, Cat. #28004) to produce tagmented DNA samples. Tagmented DNA was barcoded with Nextera Index Kit v2 (Illumina, Cat. #FC-131-2001) and amplified via PCR prior to an SPRI Bead cleanup to yield purified DNA libraries.

The ATAC-seq libraries were clustered on two lanes of a flowcell. After clustering, the flowcell was loaded on the Illumina HiSeq instrument (4000 or equivalent) according to manufacturer's instructions. The samples were sequenced using a 2x150bp Paired End (PE) configuration. Image analysis and base calling were conducted by the HiSeq Control Software (HCS). Raw sequence data (.bcl files) generated from Illumina HiSeq was converted into fastq files and de-multiplexed using Illumina's bcl2fastq 2.20 software. One mismatch was allowed for index sequence identification.

After investigating the quality of the raw data, sequencing adapters and low-quality bases were trimmed using Trimmomatic 0.38. Cleaned reads were then aligned to reference genome mm10 using bowtie2. Aligned reads were filtered using samtools 1.9 to keep alignments that (1) have a minimum mapping quality of 30, (2) were aligned concordantly, and (3) were the primary called alignments. PCR or optical duplicates were marked using Picard 2.18.26 and removed. Prior to peak calling, reads mapping to mitochondria (mt) were called and filtered, and reads mapping to unplaced contigs were removed.

MACS2 2.1.2 was used for peak calling to identify open chromatin regions. Valid peaks from each group or condition were then merged and peaks called in at least 66% of samples were kept for downstream analyses. For each pairwise comparison, peaks from condition A and condition B were merged and peaks found in either condition were kept for downstream analyses. Reads falling beneath peaks were counted in all samples, and these counts were used for differential peak analyses using the R package Diffbind.

For the differential peak analysis, peaks identified in each condition were merged, and the resulting consensus peaks were used exclusively for differential peak analyses. Reads aligning to consensus peaks were counted in all samples. Read counts in merged peaks were used to calculate distances between samples and generate a heatmap of sample-to-sample relationships. The R package DiffBind was used for differential region of interest (ROI) detection using FDR $\leq$ 0.05 as a cutoff. Peaks that have a fold-change below zero and FDR $\leq$ 0.05 indicate regions with lower accessibility. Peaks with a fold change greater than zero and FDR $\leq$ 0.05 indicate regions with higher accessibility. Peaks were annotated based on genomic features they overlapped. When annotations overlap, assignment priorities are: Promoter >5'UTR >3'UTR > Exon > Intron > Downstream > Intergenic.

For RNA-seq, total RNA was first purified from ER-HOXA9 cells using Trizol extraction according to manufacturer's instructions (Thermo Fisher). Integrity of total RNA was assayed using RNA ScreenTape

(Agilent), and mRNA was enriched with magnetic beads and RNA-seq libraries were prepared according to manufacturer's instructions (New England Biolabs). Final library sizes were confirmed with High Sensitivity D1000 ScreenTape (Agilent) and pooled for sequencing using NextSeq 550 (Illumina). RNA-seq data was aligned to the mouse genome (mm10) using STAR algorithm (Dobin et al., 2013). Differential analysis of RNA expression was performed using deepTools software (Ramírez et al., 2016).

Wright-Giemsa staining

Cells were stained with Wright-Giemsa reagent (Richard-Allan Scientific) as described elsewhere (Sykes et al., 2016). Images were acquired on a Nikon Eclipse 80i microscope with a Nikon DS-Ri1 camera using a 60× objective (with zoom knob set at 2×) for effective magnification of 120×.

RNA/DNA analysis by liquid chromatography-mass spectrometry

Total RNA was isolated from cells using Trizol (ThermoFisher). Approximately 1 microgram of total RNA was digested with 0.5 units P1 nuclease (New England Biolabs) for 2 hr at 37°C. Digested RNA was dephosphorylated with 1 unit shrimp alkaline phosphatase (New England Biolabs) for 1 hr at 37°C. Samples were syringe-filtered with a 0.22μm Durapore PVDF membrane (EMD Millipore) and autosampler loaded onto an XDB-C18 column (5cm length, 1.8μm particle size, Agilent). Analytes were resolved using a methanol gradient, with Buffer A as 99.9% water (Fisher Scientific, Optima LC-MS grade) + 0.1% formic acid (Fisher Chemical) and Buffer B as 99.9% methanol (Fisher Scientific, Optima LC-MS grade) + 0.1% formic acid, at a slope of 2–14% B from 0 to 2 min at 0.5mL/min. Analytes were analyzed on an Agilent 6470 triple quadrupole mass spectrometer operating in positive ion mode. Guanosine was detected with an MRM transition of 284.1 to 152.1 m/z, fragmentor of 70V and collision energy of 7V. Adenosine was quantified with an MRM transition of 268.1 to 136.1 m/z, fragmentor of 90V and collision energy of 14V. Thioguanosine was detected with an MRM transition of 300.1 to 168 m/z, fragmentor of 90V and collision energy of 16V. The retention time for thioguanosine, at approximately 1.2–1.3 min, was confirmed using a standard (Carbosynth).

Total genomic DNA was isolated from cells using a Purelink spin-column (ThermoFisher) and treated with Degradase Plus enzyme cocktail (Zymo Research) for 2 hr at 37°C. Samples were syringe filtered and resolved with a methanol gradient with the same conditions as described above, except at a slope of 2–20% B from 0 to 3 min. Deoxyguanosine was detected with an MRM transition of 268.1 to 152.1 m/z. Deoxyadenosine was detected with an MRM transition of 252.1 to 136 m/z. Deoxycytidine was detected with an MRM transition of 228.1 to 112.1 m/z. 5-hydroxymethyl-deoxycytidine was detected with an MRM transition of 242.1 to 126.1 m/z. Deoxythioguanosine was detected with an MRM transition of 284.1 to 168.1 m/z. All DNA-derived analytes were analyzed with fragmentor and collision energy of 90V and 16V respectively. The retention time for deoxythioguanosine, at approximately 1.4–1.6 min, was confirmed using a standard (Carbosynth).

Drug stability assays

Drugs were added to media with an initial cell density of 1×10^4 cells/ml or in mouse plasma for incubation at 37°C. Proteins were precipitated as described (Kalin et al., 2018). Analytes were resolved on a methanol gradient with the same aforementioned conditions, except the slope was 2–18% B from 0 to 2 min, 18–50% B from 2 to 2.5 min, and 50–98% B from 2.5–5 min. GSK-LSD1 was quantified with the MRM transition 217–162 m/z, fragmentor of 110V and collision energy of 20V. Mercaptopurine was quantified with the MRM transition 153–119 m/z, fragmentor of 120V and collision energy of 25V. Cerulenin was quantified with the MRM transition 224.1–179.1 m/z, fragmentor of 105V and collision energy of 5V. Retention times for GSK-LSD1, mercaptopurine, and cerulenin were 0.65–0.85, 0.75–0.95, and 3.6–3.8 min respectively.

Proliferation assay for PDX *ex vivo* cultures

For PDX AML cell proliferation assays, CellTiter-Glo Luminescent Cell Viability reagent (Promega) was used to determine the viably cell number every day according to the manufacturer's protocol. Proliferation assays were performed in triplicate and statistical significance was assessed by two-tailed Student's t-test assuming unequal variance.

Metabolome analysis

Approximately $2.5–5\times10^6$ ER-HOXA9 cells were centrifuged at 120×g, washed with ice-cold 140mM NaCl solution, centrifuged and frozen in liquid nitrogen. Metabolites were extracted as described

(Yao et al., 2020). To summarize, D8-phenylalanine (Cambridge Isotope Laboratories) was added to each cell pellet at a final concentration of 2μM as an internal standard. Cells were sonicated in methanol:chloroform:water solvent (1:1:1 volume). After centrifugation at 2000×g, the aqueous and organic layers containing polar and non-polar analytes respectively were separated and evaporated under nitrogen. Polar and non-polar analytes were resuspended in acetonitrile:water (1:1 volume) or methanol:water (9:1 volume) solvent, respectively, at volumes normalized to initial cell numbers.

Polar analytes were resolved with a pHILIC column (15cm length, 5μm particle size, HILICON) coupled to a Thermo Scientific SII UPLC system with the following conditions: Buffer A as 99.9% water with 20mM ammonium carbonate and 0.1% NH_4OH, Buffer B as 100% acetonitrile for negative ion mode detection. The gradient for polar analytes ran from 95% to 50% B from 0 to 15 min, 50%–20% B from 15 to 20 min at a flow rate of 150μL/min. Non-polar analytes were resolved with a C18 column (15cm length, 2.6μm particle size, Phenomenex) with the following conditions: Buffer A as 99.9% water with 0.1% formic acid, Buffer B as 90% isopropanol with 10% methanol. Buffer A was adjusted to either pH 4.5 or 7.4 with acetic acid or NH_4OH respectively for positive or negative ion mode detection. The gradient for non-polar analytes ran from 5 to 100% B from 0 to 20 min and maintained at 100% B from 20 to 25 min at a flow rate of 200μL/min. Metabolites were detected on a Q-Exactive HF-X Orbitrap mass spectrometer coupled to an ESI source (Thermo). We supported the identification of polar metabolites by comparing retention times to available standards and MS2 fragmentation patterns to spectra from online databases (Wishart et al., 2018).

Gene expression qPCR analysis

RNA was isolated from cells using Trizol (ThermoFisher) and quantified by Nanodrop (ThermoFisher). Approximately 0.5–1.0μg of RNA was reverse-transcribed into cDNA using PrimeScript RT (Takara) in a 10–20μL volume. For real-time amplification, cDNA was incubated with primers (ThermoFisher) and PowerUp SYBR green (Applied Biosystems) (Table S18). Extraction of RNA, reverse transcription, and amplification with reagents were done according to the respective manufacturers' instructions. Reactions were analyzed on a QuantStudio 3 thermocycler (Applied Biosystems) running the following program: 50°C for 2 min, 95°C for 3 min, 40 cycles of 95°C for 15 s and 60°C for 60 s. Relative gene expression was calculated based on the delta-delta Ct method.

QUANTIFICATION AND STATISTICAL ANALYSIS

Statistical analysis for significance

We tested whether sample groups had equal variance and were drawn from a normally distributed population using Levene and Shapiro-Wilk tests respectively. We then applied either a one-way ANOVA or Kruskal-Wallis test to compare differentiation or proliferation response across multiple treatment groups. If a difference was detected, we applied Tukey or Games-Howell post-hoc tests respectively to identify which pairs of treatment groups were significantly different from each other. Statistical tests were conducted in R (version 4.0) with the "tidyverse" (version 1.3.0) and "rstatix" (version 0.5.0) packages.

Mathematical modeling

Synergy between LSD1i and 6MP or LSD1i and CER was tested using ANOVA tests that rely on a Bliss interaction to model the proportion of non-differentiated cells among all live cells at each combination of drug concentrations according to the following definition $S_A \times S_B = S_{AB}$, where the term S_i is the proportion of surviving or live non-differentiated cells after treatment with i^{th} drug (A or B) (Demidenko and Miller, 2019). Using the Bliss model, the null hypothesis of zero or additive interaction was tested using the test statistic T given by the following equation.

$$T = \frac{\left(\overline{y}_1 + \overline{y}_2 - \overline{y}_0 - \overline{y}_3\right)\sqrt{\sum_{i=0}^{3} n_i - 4}}{\sqrt{\sum_{i=0}^{3}\sum_{j=1}^{ni}\left(y_{ij} - y_i\right)^2 \sum_{i=0}^{3} n_i^{-1}}}.$$

The framework for our test at each dose combination follows: let $y_{ij} = \mu_i + \varepsilon_{ij}$ be the log-proportion of viable cells for the j^{th} replicate in treatment i = 0,1,2,3, where 0 is no drug, 1 is LSD1i only, 2 is 6MP or CER only, and 3 is combination. The term μ_i represents the mean log-proportion in i^{th} treatment and ε_{ij} is the

measurement error of the j^{th} sample. Under the null hypothesis, the test statistic follows a t-distribution with 20 degrees of freedom. Bonferroni correction was used to adjust for family-wise error rate.

Rates of cell proliferation, death, and differentiation induced by the drugs were estimated using the ESTIpop package, with the exception that $\alpha 2$ was assigned a low number prior to the modeling (Roney et al., 2020). Rates under LSD1i treatment were assumed to be constant over time *in vitro*, while rates over time under 6MP treatment were modeled with piecewise-defined functions over time *in vitro*. A landscape for each parameter based on a B-spline basis matrix was created to predict these rates at a given combination of drug concentrations (Hastie, 1992).

Published murine pharmacokinetic (PK) models were used to predict drug concentrations of LSD1i and 6MP over time under any given regimen (Mohammad et al., 2015) (Klés et al., 2003). The LSD1i PK model relied on a one-compartment model that starts at the C_{max} with fast absorption kinetics. To generate the 6MP PK model, a modified-effect compartment was added; such a compartment is a scaled and shifted function of the drug concentration in the effect compartment to use as input for estimating proliferation and differentiation rates. The reported lag-time of 33 hr was used to shift the drug concentration in the effect compartment. Lastly, the estimated rates from the landscape fit with the concentrations from the PK models were used as inputs to simulate tumor growth and differentiation kinetics.

ADDITIONAL RESOURCES

This study was not part of a clinical trial and did not generate or contribute a new forum.